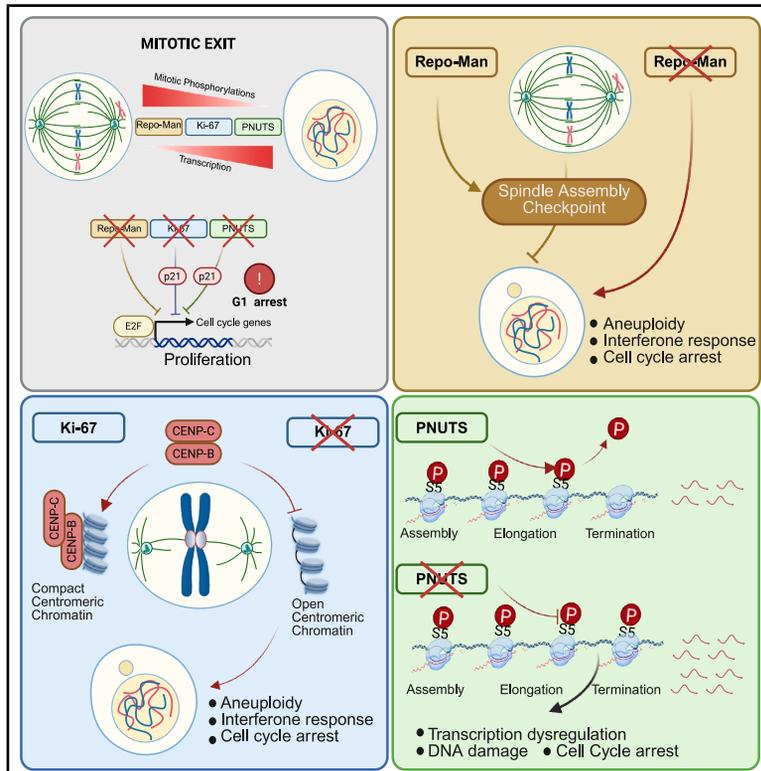# Developmental Cell

Multi-omic analyses reveal a differential contribution of chromatin-associated PP1 holoenzymes to mitotic exit and G1 re-establishment

Graphical abstract

Authors

Konstantinos Stamatiou,
Florentin Huguet, Marta Budzinska, ...,
Christos Spanos, Juri Rappsilberg,
Paola Vagnarelli

Correspondence

paola.vagnarelli@brunel.ac.uk

In brief

Stamatiou et al. combine rapid auxin-mediated degradation with multi-omics to dissect the chromatin-associated PP1 holoenzymes Repo-Man, Ki-67, and PNUTS during mitotic exit. The study uncovers non-overlapping functions in mitotic checkpoint control, centromere integrity, and transcriptional re-activation, revealing how each complex safeguards the transition into a functional G1 nucleus.

Highlights

- Multi-omic profiling uncovers divergent PP1-holoenzyme functions at the M-to-G1 transition

- Repo-Man loss accelerates mitotic exit by weakening SAC signaling

- Ki-67 depletion disrupts centromere compaction and CENP-B/C loading

- PNUTS degradation increases RNA Pol II-S5 phosphorylation, R-loops, and DNA damage

CellPress

Developmental Cell

CellPress
OPEN ACCESS

Resource

Multi-omic analyses reveal a differential contribution of chromatin-associated PP1 holoenzymes to mitotic exit and G1 re-establishment

Konstantinos Stamatiou,[1] Florentin Huguet,[1] Marta Budzinska,[1] Jose I. de las Heras,[2] Denise Ragusa,[1] Ines J. deCastro,[1] Christos Spanos,[2] Juri Rappsilberg,[2,3] and Paola Vagnarelli[1,4,*]

[1]College of Health, Medicine and Life Science, Brunel University of London, London, UK
[2]Discovery Research Platform for Hidden Cell Biology, University of Edinburgh, Edinburgh, UK.
[3]Technische Universitat Berlin, 13355 Berlin, Germany
[4]Lead contact
*Correspondence: paola.vagnarelli@brunel.ac.uk
https://doi.org/10.1016/j.devcel.2026.02.016

SUMMARY

Mitotic exit is an important part of the cell cycle, requiring the coordination of many chromatin and cytoskeleton remodeling events to successfully complete cell division and maintain cell identity. Protein dephosphorylation is a key step in directing mitotic exit, and protein phosphatase 1 (PP1) is essential to this process; however, the specific contribution of its numerous targeting subunits is still unknown. Here, we have investigated the function of three chromatin-associated PP1-targeting subunits in mitosis exit: Repo-Man, Ki-67, and protein phosphatase 1 nuclear targeting subunit (PNUTS). We generated endogenously tagged, auxin-degradable alleles for each subunit in the human cell line HCT116 and used a multi-omic approach to address their specific contributions toward transcription resumption, chromatin accessibility, and protein dephosphorylation at the transition from mitosis to G1. This approach identified their distinct role in mitotic exit, provided datasets for the cell-cycle community, and highlighted functions for Ki-67 and Repo-Man in genome stability and organization.

INTRODUCTION

When cells exit mitosis, a complex but coordinated series of morphological and biochemical changes occur to re-establish a functional G1 nucleus that is ready for the next cell cycle or differentiation. Chromatin reorganizes into the interphase form, where topologically associated domains (TADs) are re-established[1] and entanglements removed: failure in the process delays the reformation of heterochromatic and euchromatic domains[2]; chromosomes reposition in their interphase configuration, and, although the molecular mechanisms are less clear, A-type and C lamins seem to play a role.[3,4]

This transition is also characterized by waves of transcription re-activation[5] mediated by the re-establishment of long-range chromatin interactions bringing enhancers close to their promoters and/or increased binding or sequential dephosphorylation of transcription factors.

Protein dephosphorylation is key to mitotic exit. In mammalian cells, protein phosphatase 1 (PP1) and protein phosphatase 2A (PP2A) orchestrate the direction of mitotic exit events. Even in the absence of anaphase-promoting complex/cyclosome (APC/C) activity or protein translation, dephosphorylation still occurs after cyclin-dependent kinase 1 (CDK1) inhibition.[6] Dephosphorylation rates correlate with the sequence characteristics of each substrate and define the specificity of the individual phosphatases.[6] PP1 is a multimeric complex composed of a catalytic subunit and one or two regulatory/targeting subunits (regulatory-interactors-of-protein-phosphatase-one, or RIPPOs), which are essential for directing the localization of phosphatase activity. Considering the complexity of mitotic exit at the chromatin level with respect to structure, positioning, and transcriptional activity, understanding how each chromatin-associated holoenzyme contributes to the process is a priority.

RNAi-based approaches identified Repo-Man (also known as cell division cycle associated 2 [CDCA2]),[7] Ki-67,[7,8] and protein phosphatase 1 nuclear targeting subunit (PNUTS)[9,10] as important chromatin-associated PP1 regulatory subunits. Repo-Man dephosphorylates histone H3 (specifically at residues T3, S10, and S28)[11–13] and lamin A-S22 during mitotic exit,[14,15] thus playing a role in re-establishing heterochromatin;[13] Ki-67 regulates heterochromatin[16,17] and pericentromeric chromatin,[18] the nucleolar positioning of the nucleolus organizer region (NOR)-containing chromosomes,[8] and inactive X chromosome (Xi) heterochromatin maintenance;[17] PNUTS is a negative regulator of the RNA polymerase II (RNA Pol II) elongation rate.[19,20] enhances chromatin de-condensation *in vitro*,[21] modulates the tumor suppressor gene retinoblastoma (Rb) and sequesters phosphatase and tensin homolog (PTEN).[22–24]
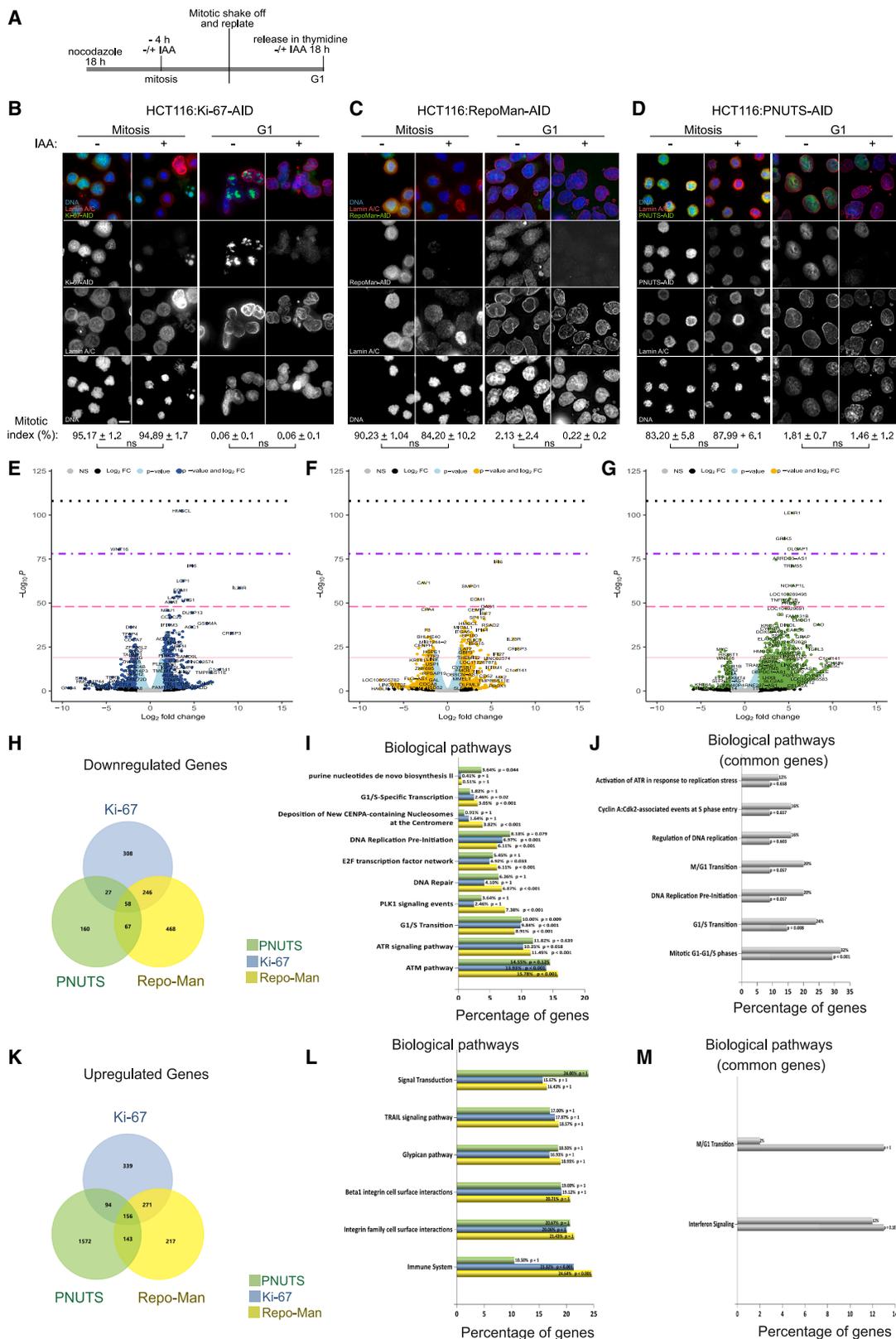
Figure 1. Unique transcriptional G1 landscape following mitotic exit without Ki-67, Repo-Man, or PNUTS

(A) Experimental scheme.

(B–D) Representative images of lamin A/C immunostaining of HCT116:Ki-67-AID (B), HCT116:Repo-Man-AID (C), and HCT116:PNUTS-AID (D) in mitosis (left) and G1 (right) ± IAA. Scale bar, 5 μm. Mitotic index is the mean ± SD, n = 3 biological replicates. Sample sizes: HCT116:Ki-67-AID (B): mitosis: control = 1,695,

(legend continued on next page)

Developmental Cell
Resource

This knowledge came from RNA interference (RNAi)-based approaches, where it was not possible to rule out that the phenotypes were consequences of defects arising from the role of these proteins in other cell-cycle stages.

We therefore embarked on dissecting the direct contribution of chromatin-associated PP1 holocomplexes in establishing the G1 nucleus by generating three HCT116 cell lines where the endogenous Repo-Man, Ki-67, or PNUTS alleles were tagged with the auxin-inducible degradation (AID) module, thus allowing for rapid protein degradation, where the consequences of a mitotic exit in the absence of each protein could be specifically evaluated. Using a multi-omic approach, we have revealed that each holoenzyme has a specific contribution to G1 establishment. Repo-Man and Ki-67 degradation lead to aneuploidy and arrest at the restriction checkpoint, whereas PNUTS degradation causes transcription misregulation. We have also unveiled additional functions for Repo-Man in sustaining the spindle assembly checkpoint, and Ki-67 in maintaining centromere integrity in mitosis.

This study improves our understanding of the function and specificity of PP1 holocomplexes at the mitosis (M)/G1 transition; it provides important datasets for these holocomplexes and sets the parameters for analyzing cell-cycle transition stages.

RESULTS

Differential contribution of Repo-Man, Ki-67, and PNUTS to the G1 transcriptional landscape

Repo-Man, Ki-67, and PNUTS are chromatin-associated RIPPOs localizing at different chromosome compartments.[7,8,12,18,25] To assess their specific contribution to the G1 nucleus establishment and discriminate between specific functions at this cell-cycle stage and secondary effects that occurred prior to mitosis, we used a Ki-67 cell line endogenously tagged with the AID degron module[26] and generated two cell lines in HCT116 where the endogenous alleles of either Repo-Man or PNUTS were tagged with mClover-AID (Figures S1A–S1I). In these cells, the addition of auxin (indole-3-acetic acid [IAA]) leads to degradation of the proteins within 3–4 h (Figures 1B–1D and S1D–S1I).

These RIPPOs load on the chromatin at different times during mitotic exit (Figures S1K–S1M), and a fraction of Repo-Man and Ki-67 accumulate in different sub-compartments at the anaphase/telophase chromosome periphery (Figure S1M). In interphase, they also occupy different chromatin regions. Analyses of published DNA adenine methyltransferase identification (DamID) datasets for Ki-67,[18,27] Repo-Man, and PNUTS[27] showed no overlaps at promoter regions (Figure S1N), and chromatin immunoprecipitation sequencing (ChIP-seq) experiments of Ki-67-AID and Repo-Man-AID at the G1/S transition (PNUTS ChIP datasets were available[28]) showed that Repo-Man-, Ki-67-, and PNUTS-bound regions cover 28.6%, 22.8%, and 12.5% of the genome, respectively (Figure S2E). Ki-67 is en-

riched at H3K9me3 chromatin blocks, as previously published[18] (Figures S2B–S2D); Repo-Man and Ki-67 are more prominent on gene-poor chromosomes, e.g., chr18, (Figure S2B), whereas PNUTS is enriched on gene-rich chromosomes, e.g., chr19 (Figure S2B). Only 3.7% of the genome is occupied by all proteins. 14.6% of regions contain both Repo-Man and Ki-67 (Figures S2F and S2G); they are H3K9me3-rich and sub-telomeric regions (Figures S2A–S2D). We previously reported this localization for Repo-Man[13] (Figure S2H), but it was never shown for Ki-67 in previous analyses.[18] The reason for the difference is unknown; however, we can exclude an artifact of the GFP antibody because GFP ChIP-seq did not reveal enrichment in the genome (Figure S2A).

As Ki-67, Repo-Man, and PNUTS chromatin localizations differ in G1, we investigated their specific contributions at the M/G1 transition and G1 chromatin landscape establishment.

The experimental setup was chosen based on previous reports on transcription resumption[5] or dephosphorylation kinetics[29] after mitosis (Figure 1A).

All cell lines blocked well in prometaphase (Figures 1B–1D, mitosis and mitotic index), and protein degradations did not affect the release (Figures 1B–1D, G1 and mitotic index). As expected, Ki-67 degradation in mitosis caused the well-described phenotype of chromosome clustering[30] (indicating that its function is required not only during chromosome condensation but also continuously during mitosis; Figure 1B, mitosis, +IAA). No obvious phenotypes of chromosome morphology were observed upon PNUTS or Repo-Man degradation (Figures 1C, 1D, mitosis, +IAA, and S3A). Upon release, all cells exited mitosis, chromosomes decondensed, and the nuclear envelope (NE) reformed (judged by lamin A/C staining) (Figures 1B–1D). We therefore conclude that, without each PP1 holoenzyme, cells can progress from mitosis to G1.

A key transition to set up the G1 nuclear landscape is an ordered transcription resumption.[5] We therefore tested how transcription was affected by the absence of each RIPPO during mitotic exit.

Following the same protocol (Figure 1A), we conducted RNA sequencing (RNA-seq). Comparisons between cell lines without IAA (RNA-seq and assay for transposase-accessible chromatin using sequencing [ATAC-seq]) showed very little differences, suggesting that the tags on the different genes have little influence (Figures S4A–S4D). However, the IAA-treated cells showed a very different and protein-specific transcriptional landscape (Figure S4A). Only 58 downregulated genes were common among the three proteins; Repo-Man and Ki-67 shared the highest number of downregulated genes, whereas PNUTS did not present many (Figures 1E–1H). Most differentially expressed genes were protein specific, indicating that gene-specificity is prominent above a general G1 nuclear disorganization response. Although Ki-67 and Repo-Man have a similar number of downregulated or upregulated genes, PNUTS behaved differently, with a high

IAA = 1,601; G1: control = 1,610, IAA = 1,705; HCT116:Repo-Man-AID (C): mitosis: control = 703, IAA = 954; G1: control = 1,191, IAA = 1,203; HCT116:PNUTS-AID (D): mitosis: control = 677, IAA = 643; G1: control = 775, IAA = 847. Chi-squared test. ns, not significant.

(E–G) Volcano plots of differentially expressed genes in G1 from the experiment in (A): HCT116:Ki-67-AID (E), HCT116:Repo-Man-AID (F), and HCT116:PNUTS-AID (G).

(H and K) Venn diagrams of downregulated (H) and upregulated (K) genes from (E)–(G).

(I and L) FunRich analysis of downregulated (I) and upregulated (L) genes from (E)–(G).

(J and M) FunRich analysis of common downregulated (I) and upregulated (L) genes from (E)–(G).
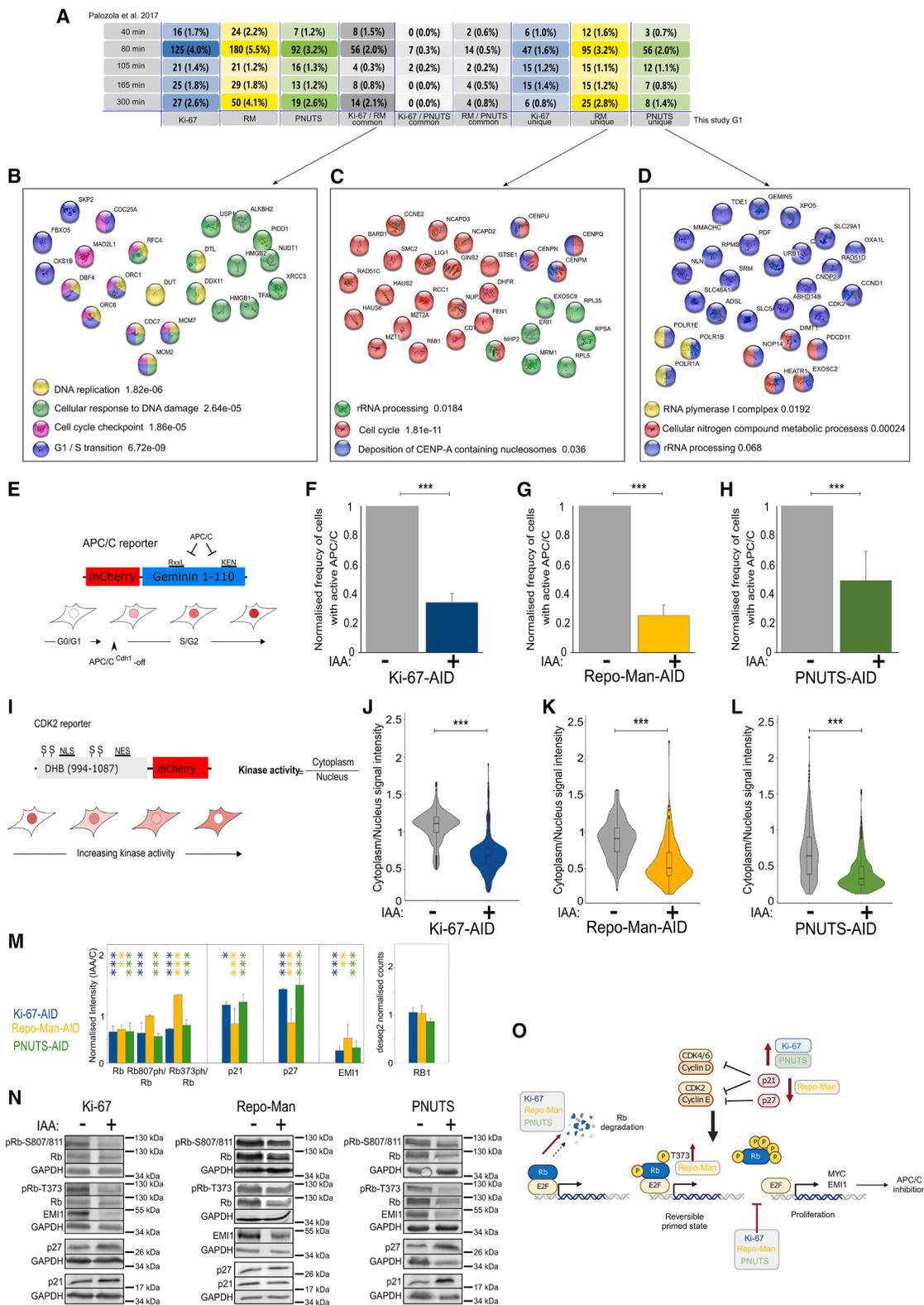
Figure 2. Mitotic exit without Ki-67, Repo-Man, or PNUTS causes G1 arrest

(A) Venn diagram of Palozola's datasets[5] (number indicates the time points) and downregulated genes of HCT116:Ki-67-AID (Ki-67), HCT116:Repo-Man-AID (RM), and HCT116:PNUTS-AID (PNUTS) cell lines; downregulated common genes of HCT116:Ki-67-AID/HCT116:Repo-Man-AID (Ki-67/RM common),

(legend continued on next page)

Developmental Cell
Resource

CellPress
OPEN ACCESS

proportion of upregulated genes (Figure 1K). This classifies the RIPPOs in two distinct categories and indicates that PNUTS is essential for a balanced transcription resumption after mitosis but does not prevent chromatin decondensation[21]—at least as assessed by microscopy, where PNUTS signal was undetectable (Figure S3A).

FunRich analyses of the dysregulated genes and their relative transcription factors revealed that "DNA replication pre-initiation" and "ataxia telangiectasia mutated (ATM) and ATR signaling pathways" were affected by Ki-67 and Repo-Man; "polo-like kinase 1 (PLK1)" and "DNA repair" were affected only by Repo-Man, and the purine *de novo* biosynthesis II pathway was affected by PNUTS (Figure 1I). The "G1/S transition" and a subset of the E2F transcription factor network were significantly downregulated in the absence of all proteins (Figures S4E–S4H); however, Reactome pathway analyses revealed that the number of genes belonging to the "G0-early G1" pathway for PNUTS was reduced compared with the other two RIPPOs; it also highlighted "cyclin D-associated events in G1"/"defective binding of RB1 mutants to E2F" and "RNA Pol III transcription termination" as PNUTS-specific enriched pathways (Figure S4O).

Repo-Man and Ki-67 share downregulated genes belonging to the "G1/S checkpoint" but also to the "activation of the pre-replicative complex" and "ATR pathway in response to replicative stress" (Figures 1I and S4M). The degradation of each protein causes the downregulation of genes transcribed by the E2F1 transcription factor, but Repo-Man and PNUTS also include genes transcribed by NFYA and SP1, respectively (Figures S4E–S4H).

Only the immune system pathway was significantly upregulated for Repo-Man and Ki-67 (Figures 1L, 1M, and S4N), with a subset of genes shared by all three RIPPOs but not significantly enriched (Figure 1M). The analyses of transcription factors for the upregulated genes only highlighted interferon regulatory factor 1 (IRF1) for Repo-Man and Ki-67, and ras-responsive element-binding protein 1 (RREB1) and hepatocyte nuclear factor 4 alpha (HNF4a) for PNUTS (Figures S4I–S4L).

These analyses strongly suggest that the three RIPPOs are essential for the re-organization of the G1 nucleus, and, in their absence, S phase cannot occur, as E2F1 targets are not expressed; nevertheless, they differ in their specificity (Figure 1J).

Lack of Repo-Man and Ki-67 during mitotic exit triggers G1 arrest at the restriction checkpoint and activation of the interferon response

To analyze the transcriptome in a timeline context and identify the stage at which transcriptional alterations occur, we cross-referenced our datasets with the transcription resumption after mitosis obtained by Palozola et al.[5] Although the experiments were conducted in a different cell line, their data suggested that cell line-specific genes are activated at later time points, making housekeeping and cell-cycle genes still a valid comparison. The intersection of the datasets shows that mitotic exit in the absence of each RIPPO affects mainly the resumption of transcription of genes activated 80 min after release (in the Palozola experimental timeline) (Figure 2A, 80 min); for Repo-Man or Ki-67, these genes belong to the G1/S transition, DNA damage, and DNA replication categories (Figure 2B).

Lack of Ki-67 does not highlight a specific pathway, whereas genes for ribosomal RNA (rRNA) processing, centromere protein A (CENP-A) deposition, and the cell cycle are Repo-Man specific (Figure 2C). Interestingly, Repo-Man is upregulated at this stage of the cell cycle,[5] which could suggest that the holo-enzyme is a key regulator of this cell-cycle transition, a function so far unknown. Lack of PNUTS affects the upregulation of the RNA Pol I complex and rRNA processing (Figure 2D).

These analyses indicate that transcription resumption at 80 min is affected when mitotic exit occurs without the PP1 holoenzymes, and strengthen the protein-specific contribution to the G1 transcription landscape.

A block in transcription resumption and E2F1 target gene downregulation strongly point toward checkpoint activation.[32]

In G1, cells make decisions about entering the cell cycle (restriction checkpoint) and committing to duplicate DNA, a process marked by APC/C inactivation and activation of CDK2/cyclin A. To address whether lack of these PP1 subunits would affect this progression, we generated cell lines on the AID background carrying reporters for APC/C^{Cdh1} (Figure 2E) or CDK2 activity (Figure 2I).[31] APC/C^{Cdh1}

HCT116:Ki-67-AID/HCT116:PNUTS-AID (Ki-67/PNUTS common), and HCT116:Repo-Man-AID/HCT116:PNUTS-AID (RM/PNUTS common); and downregulated unique genes of HCT116:Ki-67-AID (Ki-67 unique), HCT116:Repo-Man-AID (RM unique), and HCT116:PNUTS-AID (PNUTS unique).

(B) String analysis of common downregulated genes HCT116:Ki-67-AID/HCT116:Repo-Man-AID/5 (B) and HCT116:Repo-Man-AID-unique/5 at the 80 min time point (C).

(D) String analysis of overlapping unique downregulated genes of HCT116:PNUTS-/5 at the 80 min time point.

(E) Schematic of the APC/CCDH1 reporter32.

(F–H) Percentage of geminin-positive/negative cells of HCT116:Ki-67-AID (F), HCT116:Repo-Man-AID (G), and HCT116:PNUTS-AID (H) from the experiment in Figure 1A. Values are the average of $n = 3$ biological replicates, and error bars represent the SD. Sample size: HCT116:Ki-67-AID: control = 1,197, IAA = 1,685; HCT116:Repo-Man-AID: control = 699, IAA = 832; HCT116:PNUTS-AID: control = 1,174, IAA = 709. Chi-squared test. ***$p < 0.001$; ns, not significant.

(I) Schematic of the CDK2 reporter.[31]

(J–L) Cytoplasmic/nuclear ratios of $n = 3$ biological replicates of the HCT116:Ki-67-AID:DHB (J), HCT116:Repo-Man-AID:DHB (K), and HCT116:PNUTS-AID:DHB (L). Sample size: HCT116:Ki-67-AID: control = 329, IAA = 310; HCT116:Repo-Man-AID: control = 164, IAA = 174; HCT116:PNUTS-AID: control = 550, IAA = 462. Wilcoxon test. ***$p < 0.001$.

(M) Quantification of the blots in (N) (left). Values represent the average of $n = 2$ biological replicates, and the error bars represent the SD. (Right) RB1 expression levels from the RNA-seq in Figures 1E–1G. Values represent the average of $n = 3$ biological replicates, and error bars are the SD. Student's t test: *$p < 0.05$, **$p < 0.01$, ***$p < 0.001$; ns, not significant.

(N) Representative western blots of the HCT116:Ki-67-AID, HCT116:Repo-Man-AID, and HCT116:PNUTS-AID cell lines following the experiment in Figure 1A. Blots were probed for pRB-S807/811, total RB, pRB-T373, total RB and EMI1, p27, p21, and GAPDH.

(O) Proposed model for the contribution of the three RIPPOs to G1 progression.
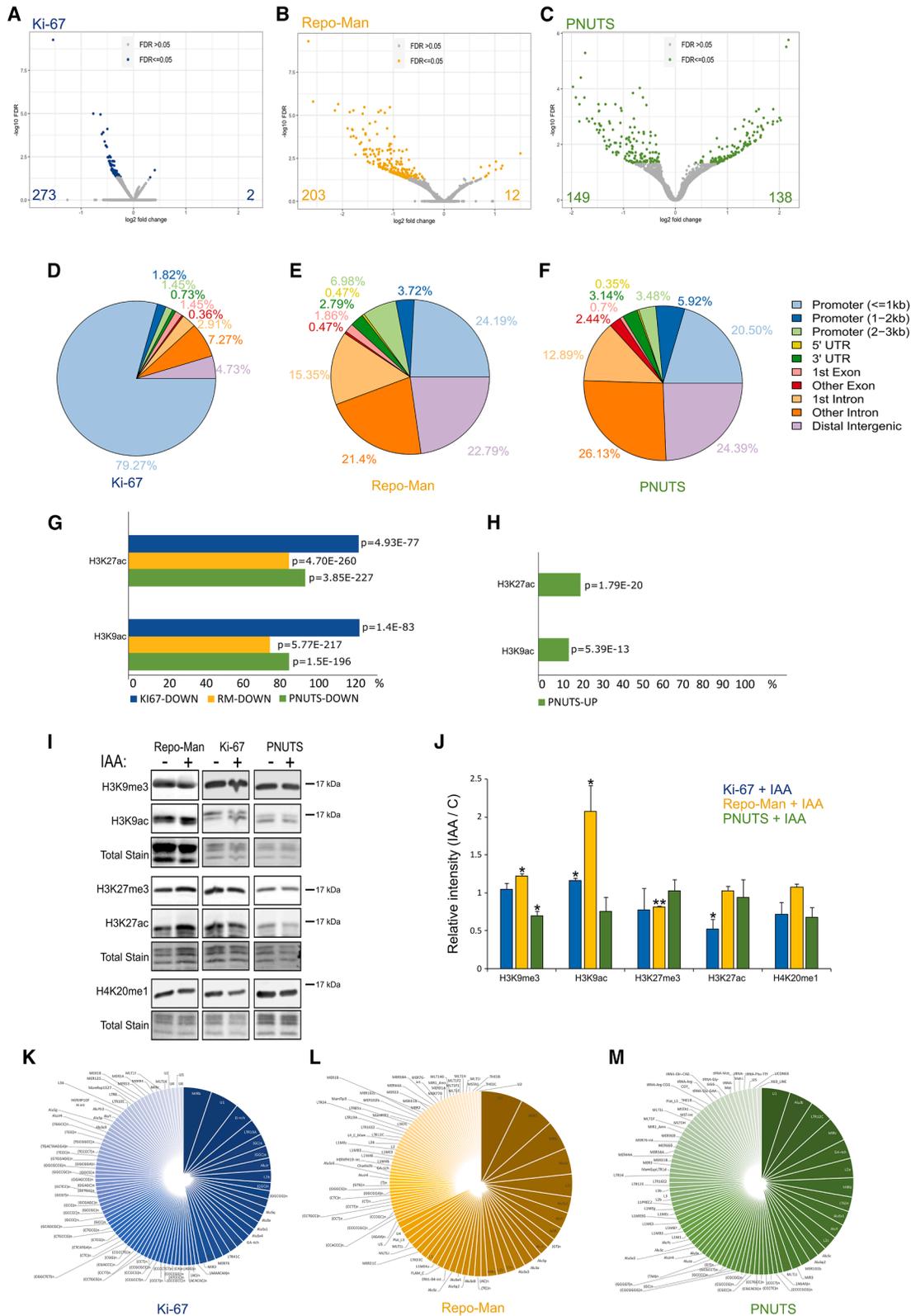
Figure 3. Mild changes in chromatin accessibility in G1 following mitotic exit without Ki-67, Repo-Man, or PNUTS

(A–H) Volcano plots (A–C) and genome-wide distribution (D–F) of differentially accessible chromatin (ATAC-seq) for the HCT116:Ki-67-AID (A), HCT116:Repo-Man-AID (B), and HCT116:PNUTS-AID (C) (experiment in Figure 1A). Accessible regions were classified as promoter (≤1, 1–2, and 2–3 kb), gene body (5′ UTR, 3′ UTR, 1st exon, other exon, 1st intron, and other intron), and distal intergenic regions. Overlaps between less (G) and more (H) accessible chromatin

(legend continued on next page)

Developmental Cell
Resource

inactivation would cause nuclear accumulation of the mCherry reporter. Cells that went through mitotic exit without each RIPPO cannot inactivate the APC/C[Cdh1] (Figures 2F–2H), albeit less so for PNUTS; this milder effect could be due to the requirement for a stronger PNUTS depletion to halt cell-cycle progression or to the very different transcriptional landscape. Activation of the CDK2 kinase leads to the accumulation of the mCherry reporter in the cytoplasm, and mitotic exit in the absence of each protein prevented CDK2 activation (Figures 2J–2L).

Western blot analyses of critical regulators of this pathway showed, for all three proteins, a decrease in total Rb (but not its transcript), possibly caused by Rb degradation upon the arrest[33] (Figures 2M and 2N). Lack of Rb phosphorylation and increases in p21 and p27 for PNUTS and Ki-67 support the G1 block (Figures 2M, 2N, and S3B–S3E). Rb hypophosphorylation upon PNUTS degradation could be compatible either with Rb being a direct PNUTS substrate or a consequence of the G1 arrest. Previous studies reported that PNUTS depletion favors Rb dephosphorylation; in vitro studies suggested that PNUTS inhibits PP1 activity toward Rb[34] by blocking its binding sites on PP1.[35] We tested whether PNUTS also restricts Rb dephosphorylation in vivo. To uncouple the effect of G1 arrest from the PP1 repressor function, we arrested cells with thymidine for 18 h (at this stage, all cells have progressed through the restriction point in G1, and Rb is fully phosphorylated), then IAA was added (Figure S3F); quantifications of the total Rb level and its phosphorylation status at the 807–811 and 373 sites showed no decrease in both total Rb and its phosphorylation levels (Figures S3G and S3H). We conclude that the major effect on Rb upon mitotic exit is the block at the restriction checkpoint and that PNUTS does not act as a PP1 repressor in cells at G1/S.

Unique to Repo-Man depletion is Rb hyperphosphorylation at its 373 residue, a signature linked to a primed G1 state during which cells remain sensitive to fluctuating signals.[36] Here, there is no increase in p21 and p27, but the APC/C early mitotic inhibitor 1 (EMI1) is decreased (Figures 2M–2O).

For Repo-Man and Ki-67, the interferon pathway activation led us to consider that chromosome mis-segregation could be the cause of the arrest, as it has been linked to the activation of the interferon response via the cGAS/STING pathway.[37] We therefore analyzed ploidy by fluorescence in situ hybridization (FISH) on interphase cells that exited mitosis, with and without each of the RIPPOs. Lack of Repo-Man and Ki-67 leads to a significant increase in aneuploid cells for both chromosomes 1 and 15; however, PNUTS did not (Figures S5D–S5F).

Lack of PNUTS also triggered an interferon response but with fewer genes involved (Figures 1M and S5A–S5C) and no aneuploidy. We hypothesized that DNA damage could contribute to interferon activation in the absence of PNUTS. Neutral COMET assay analyses showed that lack of Repo-Man, Ki-67, and

PNUTS causes a significant increase in DNA damage (Figures S5G–S5J). Moreover, lack of PNUTS also leads to hyperphosphorylation of proteins important for the DNA damage response (namely TP53BP,[38] FANCD,[39] and RAP80[40,41]) (differential phosphoproteomic datasets—see later in the text) (Figure S5M).

Aneuploidy triggers nuclear deformation as well as lamin and heterochromatin alterations, leading to rapid p53/p21 activation upon mitotic exit.[42] Repo-Man does not seem to trigger this pathway, even if we have shown that its depletion causes aneuploidy, nuclear envelope (NE) and heterochromatin defects.[12–14] Because of the link between Repo-Man and the NE, it would be important to understand whether the protein represents an effector for this signaling cascade.

Ki-67 degradation leads to upregulation of genes involved in the mesenchymal-to-epithelial transition pathway (Figure S5K) and genes transcribed by Fos and Jun (Figure S5L). Previous work showed that cells lacking Ki-67 do not metastasize,[43–46] and our finding suggesting a reversal of the aggressive phenotype of cancer cells could be important for considering this marker not only as a bystander of proliferation but also as a cancer target.

Chromatin accessibility and epigenetic marks only partially correlate

These proteins have been linked to chromatin organization; therefore, their absence could cause chromatin alterations contributing to the transcriptional changes observed in G1. Analyses of chromatin accessibility of G1 nuclei by assay for transposase-accessible chromatin using sequencing (ATAC-seq) and immunoblotting for histone modifications (Figure 1A) revealed changes within the chromatin, but these were less pronounced than those observed for transcription. Ki-67 or Repo-Man decreased chromatin accessibility (273 and 203 regions, respectively) (Figures 3A, 3B, S4C, and S4D); PNUTS presented changes in both directions (149 regions less accessible and 138 more open) (Figure 3C). For Repo-Man and PNUTS, 84% of the regions are within promoters (less than 1 kb), distal intragenic regions, and introns (Figures 3E and 3F); for Ki-67, 79% are located within the proximal promoters (less than 1 kb) (Figure 3D). Regions that become less accessible are enriched for the open chromatin marks H3K9ac and H3K27ac, which are also significantly enriched in accessible regions following PNUTS degradation (Figures 3G and 3H).

Immunoblotting analyses of chromatin isolated by micrococcal nuclease digestion showed an increase in H3K9ac and a decrease in H3K27me3 (Figures 3I and 3J) for Repo-Man. Although bulk chromatin fraction analyses by western blot do not provide a granular picture, these observations are congruent with previous findings. For example, the Van Steensel group[18] showed only subtle changes in H3K27me3 (we see a modest overall change) and H3K9me3 (we do not see any changes)

regions (ATAC-seq) for the HCT116:Ki-67-AID, HCT116:Repo-Man-AID, and HCT116:PNUTS-AID cell lines in G1, and HCT116 H3K9ac or H3K27ac ChIP-seq datasets (ENCODE) (Fisher exact test p values).
(I) Representative western blots of micrococcal-digested chromatin for HCT116:Ki-67-AID, HCT116:Repo-Man-AID, and HCT116:PNUTS-AID cell lines in G1 (Figure 1A). Blots were probed for H3K9me2, H3K9ac, H3K27me3, H3K27ac, and H4K20me1 and stained with total protein stain.
(J) Quantification of the blots in (I). Values represent the average of n = 3 biological replicates, and the error bars represent the SD. Student's t test. *p < 0.05, **p < 0.01; ns, not significant.
(K–M) Overlaps between less-accessible chromatin regions (ATAC-seq) for the HCT116:Ki-67-AID (K), HCT116:Repo-Man-AID (L), and HCT116:PNUTS-AID (M) cell lines in G1 (Figure 1A) and repeat DNA sequences.
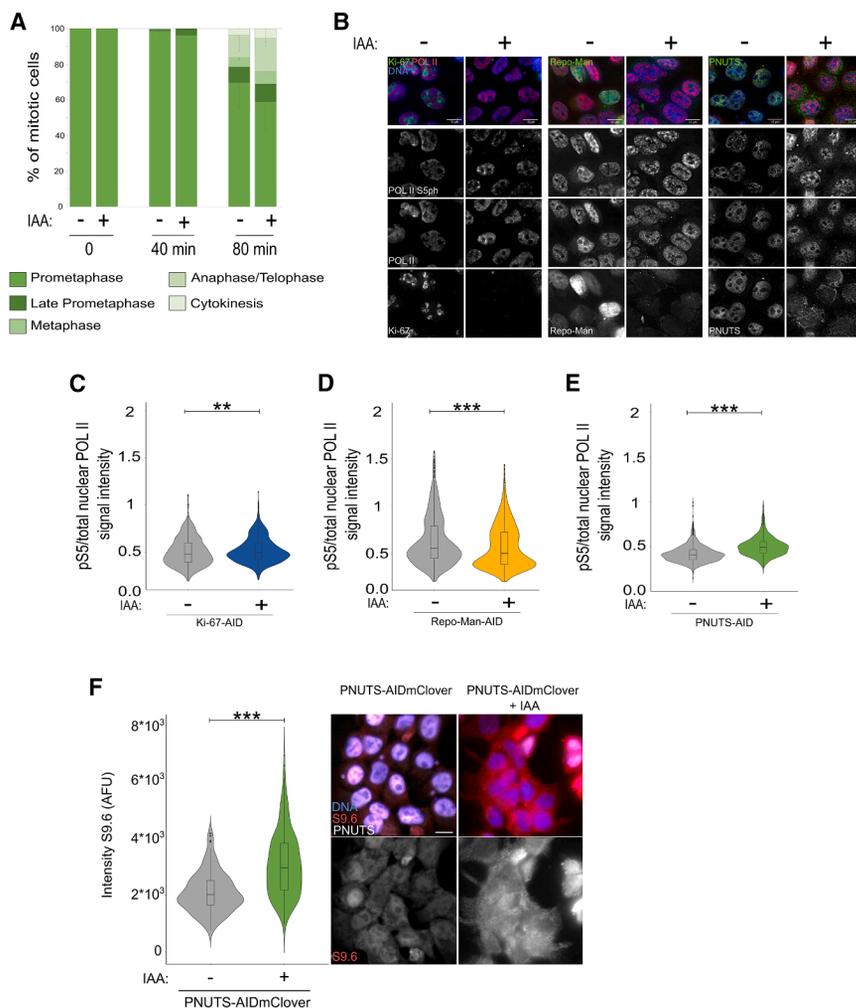
Figure 4. PNUTS is a major regulator of transcription in G1

(A) Quantification of mitotic stages at 0, 40, and 80′ post release from nocodazole ± IAA (as in Figure 1A). Sample size: control: 0 = 300, 40 = 315, and 80 = 322; IAA: 0 = 303, 40 = 257, and 80 = 354.

(B) Representative images of RNA Pol II (POLII) and RNA Pol II (S5ph) immunostaining on HCT116:Ki-67-AID, HCT116:Repo-Man-AID, and HCT116:PNUTS-AID cell lines, treated as in Figure 1A. Scale bar, 10 μm.

(C–E) RNA Pol II S5ph/total RNA Pol II fluorescence intensity ratio of HCT116:Ki-67-AID (C), HCT116:Repo-Man-AID (D), and HCT116: PNUTS-AID (E) cell lines. Wilcoxon test. **$p < 0.01$, ***$p < 0.001$.

(F) Representative images of HCT116:PNUTS-AID cells treated as in Figure 1A and immunostained with anti-S9.6 antibody. Scale bar, 5 μm (right). Quantification of the experiment (left); sample size: control = 184, IAA = 261. Wilcoxon test. ***$p < 0.001$.

presses transcription/replication (T-R) conflicts by promoting degradation of RNA Pol II on chromatin and reducing its residence time.[19] We have analyzed cells in G1, before replication commences, and we still observe an aberrant transcription landscape with almost 2,000 upregulated genes (Figure 1L). A significant increase in nuclear RNAPIIS5ph was found upon PNUTS degradation; this supports PNUTS' involvement in RNA Pol II phospho-regulation, where its absence causes genome-wide acceleration of transcription, previously shown to be PP1 dependent.[48] A decrease in RNAPIIS5ph is observed upon Repo-Man degradation, consistent with halted transcription resumption, but no changes occurred without Ki-67 (Figures 4B–4E).

Transcription termination defects caused by RNA Pol II removal have been associated with R-loop formation and genome instability.[51–53] This could explain why cells without PNUTS have increased damage and hyperphosphorylation of DNA damage response proteins, a possible trigger for the interferon response (Figures S5G, S5J, and S5M). Using the DNA-RNA hybrid-specific S9.6 antibody, widely employed to detect R-loops,[54] we found a significant increase in the intensity of S9.6 upon PNUTS degradation (Figure 4F).

These data suggest that PNUTS is a major regulator of transcription in G1; its degradation at this cell-cycle transition leads to uncontrolled gene expression, possibly contributing to DNA damage and preventing G1/S progression via p21 and Rb dephosphorylation.

distributions following acute Ki-67 depletion in HCT116 cells. We previously showed that Repo-Man RNAi reduces H3K27me2/3 at some polycomb targets and that recruitment of Repo-Man to chromatin increases H3K9 acetylation.[13] All these are consistent with our findings using this system.

Lack of Ki-67 significantly decreases H3K27ac and increases H3K9ac, while PNUTS shows only a decrease in H3K9me2 (Figures 3I and 3J). Whereas for Ki-67, the changes could be related to a shift toward the more closed chromatin observed by ATAC-seq and downregulation of several genes, for Repo-Man, increased acetylation (H3K9ac) does not translate into more open chromatin (at least as judged by ATAC-seq). The analyses of repeated elements within the altered regions did not reveal any significant enrichments (Figures 3K–3M).

PNUTS is a major regulator of transcription in G1

RNA-seq and ATAC-seq analyses show that PNUTS greatly affects transcription and chromatin accessibility (Figures 1G, 1H, 1L, and 3C). These data agree with studies suggesting PNUTS' involvement in transcription regulation[20,47,48] but do not support PNUTS' role in exiting mitosis, as previously proposed.[49]

PNUTS' only established substrate is Ser5 in the CTD of RNA Pol II (pRNAPII S5),[47,50] whereby its dephosphorylation sup-

Differential phosphoproteomic analyses reveal non-overlapping functions for the three PP1 holocomplexes

Exiting mitosis is also accompanied by major dephosphorylation, triggered by the inhibition of mitotic kinases and the
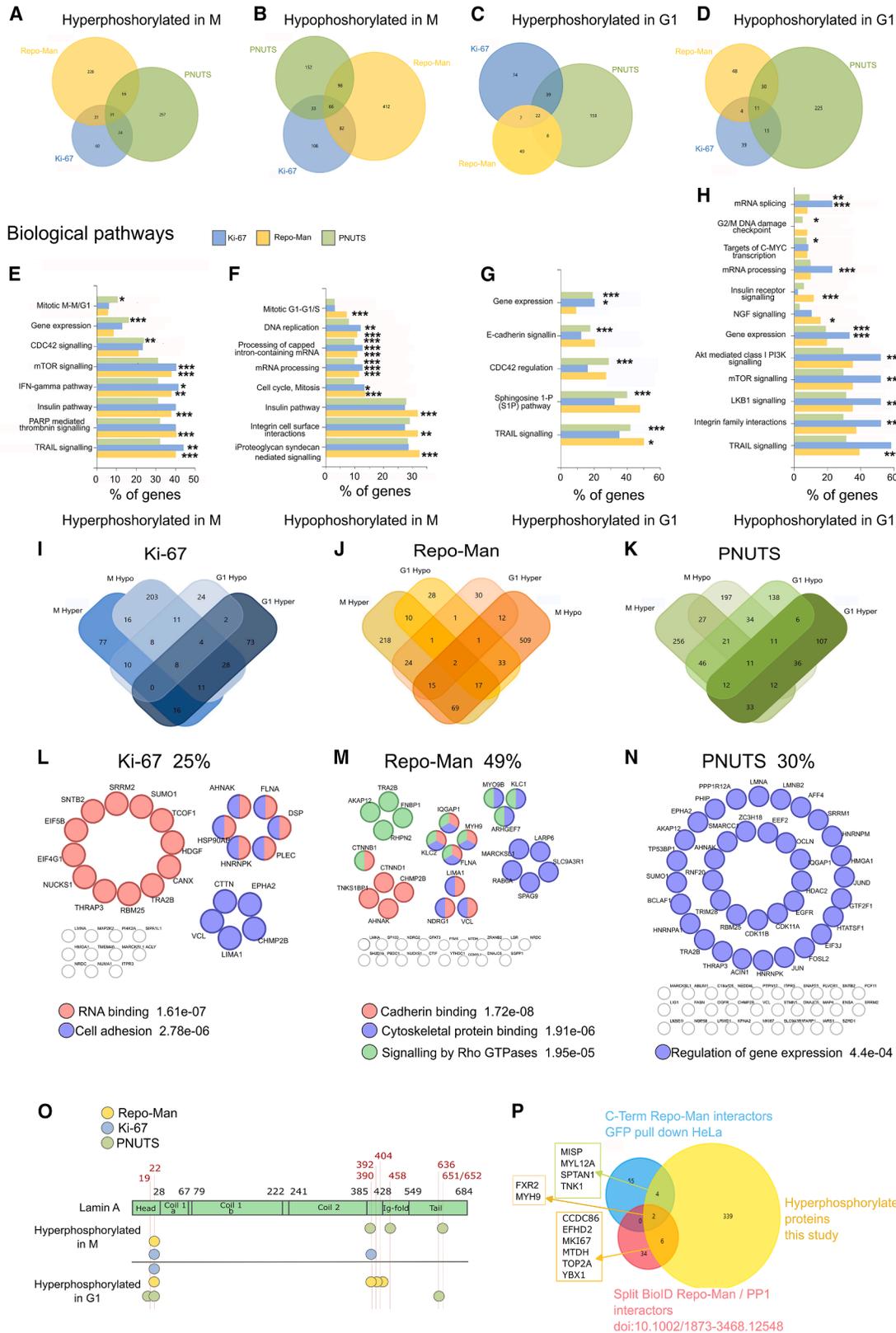
Figure 5. Differential phospho-proteomics in G1 reveal changes unique for each RIPPO

(A–D) Venn diagrams of differentially hyperphosphorylated (A and C) or hypophosphorylated (B and D) proteins in mitosis (A and B) or G1 (C and D).

(E–H) FunRich analysis of hyperphosphorylated (E and G) and hypophosphorylated (F and H) proteins in mitosis (E and F) or G1 (G and H).

(legend continued on next page)

activation of protein phosphatases.[55] Repo-Man and Ki-67 bind to PP1 more strongly and more stably after anaphase onset,[8,12,56] and Repo-Man/PP1 has been shown to have several chromosome substrates, including H3T3, H3S10, H3S28[11–13] and lamin A S22,[14] whereas Ki-67/PP1 seems only to dephosphorylate itself.[57] We therefore investigated the differential phosphoproteomes both in mitosis and G1 cells after the degradation of these PP1 holoenzymes. Nocodazole-arrested (18 h) cells ± IAA (4 h) were SILAC labeled; mitotic cells were fractionated into chromatin and nucleoplasmic fractions (Figures S6A and S6B) and processed for mass spectrometry, with and without phospho-enrichment. Other cell samples were released from the nocodazole block in medium containing thymidine and collected at the same time point as the previous RNA-seq and ATAC-seq experiments.

Differentially phosphorylated protein analyses (cutoffs -0.83 and $+1.3$ H/L ratios) revealed little overlap between the three RIPPOs, with Repo-Man and PNUTS sharing the highest number of hypo- and hyperphosphorylated proteins (Figures 5A–5D). Proteins involved in gene expression processes become hyperphosphorylated in M mainly upon PNUTS degradation, a finding that aligns with the transcription misregulation observed; mTOR, TNF-related apoptosis-inducing ligand (TRAIL) signaling, and interferon pathway proteins are hyperphosphorylated following Repo-Man and Ki-67 degradation, whereas the insulin pathway is unique to Repo-Man (Figure 5E). This category of hyperphosphorylated proteins is interesting because it contains mitotic substrates.

Proteins that become dephosphorylated in mitosis show more overlaps in terms of biological pathways, and all three RIPPOs affect proteins involved in DNA replication and RNA processing. Lack of Repo-Man seems to trigger the dephosphorylation of proteins involved in the cell cycle, the transition from mitosis to G1, and, again, the insulin pathway (Figure 5F). When the analysis is conducted for proteins differentially phosphorylated in G1, PNUTS is the only RIPPO that leads to a significant enrichment in a few categories, including gene expression and CDC42 regulation (Figure 5G). For the hypophosphorylated proteins, PNUTS affects the phosphoregulation of transcription processes, including C-MYC targets, whereas Repo-Man affects the insulin signaling (Figure 5G). These findings suggest a dominant role for PNUTS in transcription regulation at this cell-cycle stage and highlight the involvement of Repo-Man in insulin pathway regulation and glucose signaling.

Hyperphosphorylated proteins in G1 should contain mitotic exit substrates of these holoenzymes; however, the hyperphosphorylation could also be the aftermath of mitotic substrates that become hyperphosphorylated before exiting mitosis and then maintain a higher phosphorylation level throughout G1. To understand how many proteins are affected this way, we analyzed the differential phospho-proteome overlaps between M and G1 for each RIPPO. Surprisingly, 25%–49% of hyperphosphorylated proteins in G1 are also hyperphosphorylated in M (Figures 5I–

5N). This observation is important and needs to be considered in future phosphoproteomic analyses when protein depletion could affect other cell-cycle stages. In this latter category, PNUTS again shows enrichment for proteins involved in transcription (Figure 5N). Ki-67 highlights cell adhesion proteins (Figure 5L), an interesting finding in light of the upregulation of MET genes (Figures S5K and S5L) and published studies in 4T1 cells.[43]

Intersecting RIPPO pull-down experiments or proximity biotinylation approaches with these differential phosphoproteomes would provide a list of highly probable substrates.[59] We conducted these analyses with Repo-Man because pull-down datasets from human cells (HeLa) and biotinylation experiments using a split BioID approach in HEK293T cell[58] are available; we identified interesting candidate substrates for Repo-Man/PP1, including myosin heavy chain 9 (MYH9—with a role in cytokinesis), topoisomerase II, Ki-67, and CCDC86 (involved in chromosome structure and segregation and an effector of KRAS signaling inhibition)[60,61] (Figure 5P). The short list reflects the power of the approach that eliminates most secondary events; however, we could have missed some substrates because pull-downs or split biotinylations cannot retrieve the full interactome. The identification of Ki-67 as a possible Repo-Man substrate is interesting and could explain why some of the changes in G1 upon Repo-Man degradation overlap with the ones found upon Ki-67 degradation.

The analyses described above mainly focus on proteins unique for each RIPPO, assuming that one holoenzyme is specific for the dephosphorylation of a single protein. However, proteins could be phosphorylated at multiple sites, and each site could also be dephosphorylated at different stages by different proteins. As an example, we have analyzed the phosphorylation status of lamin A because it appears in all the samples, and it is also a Repo-Man substrate.[14,15] Several lamin A sites become hyperphosphorylated in mitosis upon degradation of each RIPPO: S22 (Ki-67 and Repo-Man)—this residue, previously identified as a Repo-Man substrate,[14,15] was confirmed by these unbiased analyses—S390 (PNUTS and Ki-67), S494 and S651 (PNUTS). In G1, T19 and S636 are only found upon PNUTS degradation; S390, S392, and S404 are only found upon Repo-Man degradation, and these sites are important for the regulation of the nuclear localization of lamin A and its polymerization[62,63] (Figure 5P). Altogether, these findings point to Repo-Man as the major lamin A phosphatase.

In summary, the comparative analyses show no redundancy among the three complexes: hyperphosphorylations in mitosis were more prominent upon Repo-Man and PNUTS degradation, whereas Repo-Man caused dephosphorylation of several proteins, possibly as downstream effects of important biological functions of Repo-Man in mitosis.

### Ki-67 maintains centromere organization at the M/G1 transition

STRING analyses of Ki-67 differential phosphoproteome in mitosis revealed a significant enrichment for chromosome

---

(I–K) Venn diagram of hyperphosphorylated and hypophosphorylated proteins in mitosis and/or G1.

(L–N) String analyses of hyperphosphorylated proteins in both mitosis and G1.

(O) Scheme of lamin A structure and domains with hyperphosphorylated or hypophosphorylated residues from the phosphoproteomics analyses.

(P) Overlaps of hyperphosphorylated proteins of the HCT116:Repo-Man-AID cell line in mitosis, GFP-Repo-Man C-term, or split BioID Repo-Man/PP1 interactors[58].
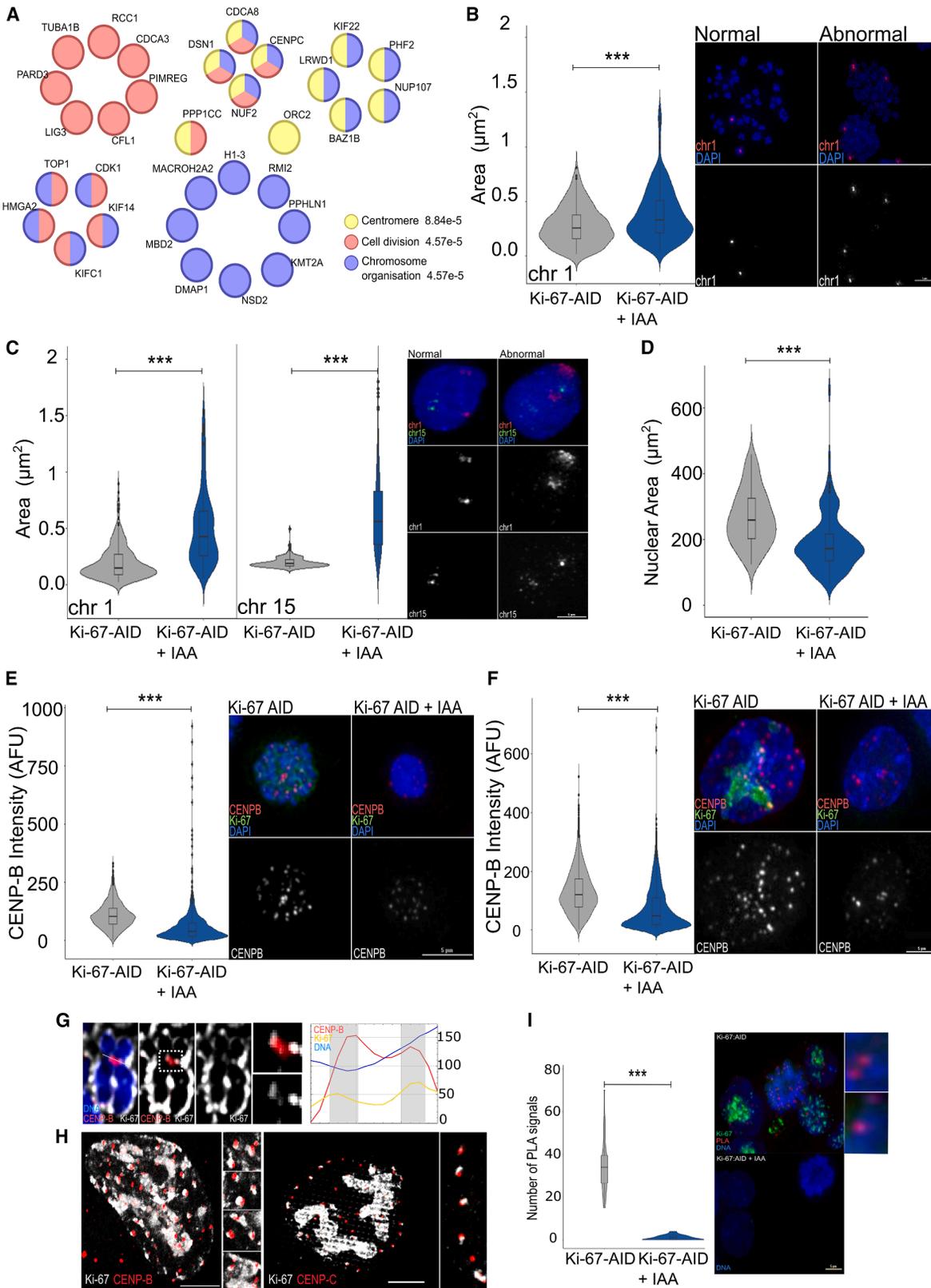
(legend on next page)

organization, cell division, and centromeric proteins (Figure 6A; Table S2); we identified phosphorylation changes for sororin (CDCA5), a protein essential for the maintenance of chromatid cohesion in mitosis;[64] survivin (CDCA3), necessary for CPC recruitment to centromeres;[65] Ndc80 kinetochore complex component (NUF2); and CENP-C, a key kinetochore component whose phosphorylation promotes kinetochore assembly.[66]

Because lack of Ki-67 during mitotic exit leads to aneuploidy, a block at the restriction checkpoint with upregulation of p21, together with previous reports showing that Ki-67 promotes timely replication[18] and organization of centromeric chromatin[26] in S phase, we investigated a link between Ki-67 and centromere organization.

Using FISH for chromosome 1 centromeric satellites, we showed that, without Ki-67, the centromeric regions are expanded (Figure 6B). Similar results were obtained from cells that exited mitosis without Ki-67 (Figure 6C), even if the nuclear area was significantly smaller (Figure 6D), ruling out a general effect of Ki-67 on chromatin compaction. No changes were observed upon degradation of Repo-Man or PNUTS (Figures S7A–S7D). Lack of CENP-B leads to centromere decompaction and an increase in centromeric area.[67] We therefore analyzed CENP-B levels and showed a decrease both in mitosis (Figure 6E) and in G1 (Figure 6F) (not linked to a decrease in CENP-B transcription, Figure S7E). Similarly, CENP-C levels (CENP-C is hypophosphorylated in mitosis without Ki-67) are also decreased in mitosis (Figure S7F) and G1 (Figure S7H) cells, although CENP-C transcription was affected in G1 (Figure S7G). Importantly, overexpression of mCherry-tagged CENP-B rescued CENP-C levels on mitotic chromosomes in the absence of Ki-67 (Figures S7I and S7J).

Ki-67 in mitosis accumulates at the periphery of the chromosomes (albeit dynamically[68]); we therefore analyzed, at higher resolution, whether Ki-67 was visible at the centromeres in mitosis and G1. In chromosome spreads, we could detect partial overlaps between Ki-67 and centromeric proteins (Figure 6G), which was confirmed by proximity ligation assays (PLAs) between endogenous Ki-67 and CENP-B (Figure 6I). In G1 cells that have not yet reformed the nucleoli, Ki-67 is present in aggregates, and CENP-B is in proximity to these localized Ki-67 clusters, which enwrap the centromeres; when analyzed by DeepSIM, we could clearly see co-localization between Ki-67

and CENP-B (Figure 6H, left). Even when the nucleoli are reformed, and after replication when Ki-67 appears at the nuclear periphery,[26] co-localization between CENP-C and Ki-67 is maintained (Figure 6H, right).

Searching for a mechanistic insight into how centromeres are compromised by Ki-67 removal, we considered the centromere epigenetics. H4K20 monomethylation (H4K20me1) is enriched at centromeres, and its reduction results in kinetochore assembly defects.[69] Recent studies showed that CENP-A containing higher order repeats (HORs) are enriched in H3K9me3.[70] Ki-67 also co-localizes with H3K9me3-enriched genomic regions (van Schaik et al.[18] and this paper; Figure S2). We therefore tested the levels of these modifications upon Ki-67 degradation when cells are arrested in mitosis. Our results show that H4K20me1, but not H3K9me3, total levels are reduced upon Ki-67 degradation (Figure S7K), potentially supporting changes in the centromere chromatin landscape. Further studies will be needed to identify the molecular details.

Cells lacking Ki-67 slightly delay chromosome alignment (Figure S7L; Cuylen et al.[71]), but all cells exit mitosis (Figures 1B and 1D, G1), although with chromosome segregation errors (Figures S5D–S5F).

These analyses led us to conclude that Ki-67 is in proximity to the centromeres, playing a key role in maintaining a compact centromere structure important for CENP-B localization and normal phosphorylation of a subset of centromeric proteins.

Repo-Man is essential for maintaining the mitotic checkpoint

Mitotic exit without Repo-Man causes aneuploidy, G1 arrest, and interferon signaling activation—but not centromeric chromatin defects (Figure S7A; Table S3).

Repo-Man-specific differential phosphoproteome revealed changes in cell cycle and mitotic proteins, together with the hypophosphorylation of several APC/C components, including cell division cycle 20 (CDC20) S41 (Figures 7A and S6D). This scenario suggests a role for Repo-Man in maintaining mitotic arrest, a function previously unknown and contrary to the current assumption that Repo-Man is inactive in mitosis and mainly needed for mitotic exit-specific dephosphorylation events.[12,72]

We tested this hypothesis by analyzing the mitotic exit progression of cells released from nocodazole. At 80 min, 70% of

---

Figure 6. Ki-67 maintains centromere organization

(A) String analysis of differentially phosphorylated proteins for Ki-67 from Figure 5B.

(B) Mitotic HCT116:Ki-67-AID cells ± IAA were subjected to FISH with a centromeric chromosome (chr) 1 probe. Representative images of normal and abnormal FISH signals (right) and quantification of the area occupied by the signals (left). Scale bar, 5 μm. Sample size: control = 194, IAA = 296. Wilcoxon test. ***$p < 0.001$.

(C) FISH of HCT116:Ki-67-AID cells treated as in Figure 1A. Examples of normal/abnormal signals obtained with the pUC177 (red signals, chr1) and pTRA-20 (green signals, chr15) (right), and quantification of the area occupied by the signals (middle and left). Scale bar, 5 μm. Sample size: CHR1: control = 280, IAA = 284; CHR15: control = 253, IAA = 235. Wilcoxon test. ***$p < 0.001$.

(D) Quantification of the nuclear area in μm^2 of HCT116:Ki-67-AID treated as in Figure 1A. Scale bar, 5 μm. Sample size: control = 95, IAA = 114. Wilcoxon test. ***$p < 0.001$.

(E) Representative images of CENP-B immunostaining of mitotic HCT116:Ki-67-AID ± IAA cells (right) and quantification of CENP-B intensity (left). Scale bar, 5 μm. Sample size: control = 2,139, IAA = 1,646. Wilcoxon test. ***$p < 0.001$.

(F) Representative images of CENP-B immunostaining of HCT116:Ki-67-AID ± (as in Figure 1A) (right) and quantification of CENP-B intensity (left). Scale bar, 5 μm. Sample size: control = 1,786, IAA = 3,985 foci. Wilcoxon test. ***$p < 0.001$.

(G) Representative images of CENP-B immunostaining on mitotic HeLa chromosomes (left) and RGB intensity plot (right). Scale bar, 5 μm.

(H) Representative DeepSIM images of HCT116:Ki-67-AID immunostained for CENP-B or CENP-C. Scale bar, 10 μm.

(I) Representative images of proximity ligation assay (PLA) with CENP-B and GFP antibodies on asynchronous HCT116:Ki-67-AID cell line ± IAA. Quantification of PLA signals in mitotic cells (left). Scale bar, 5 μm. Sample size: control = 36, IAA = 22. Wilcoxon test. ***$p < 0.001$.
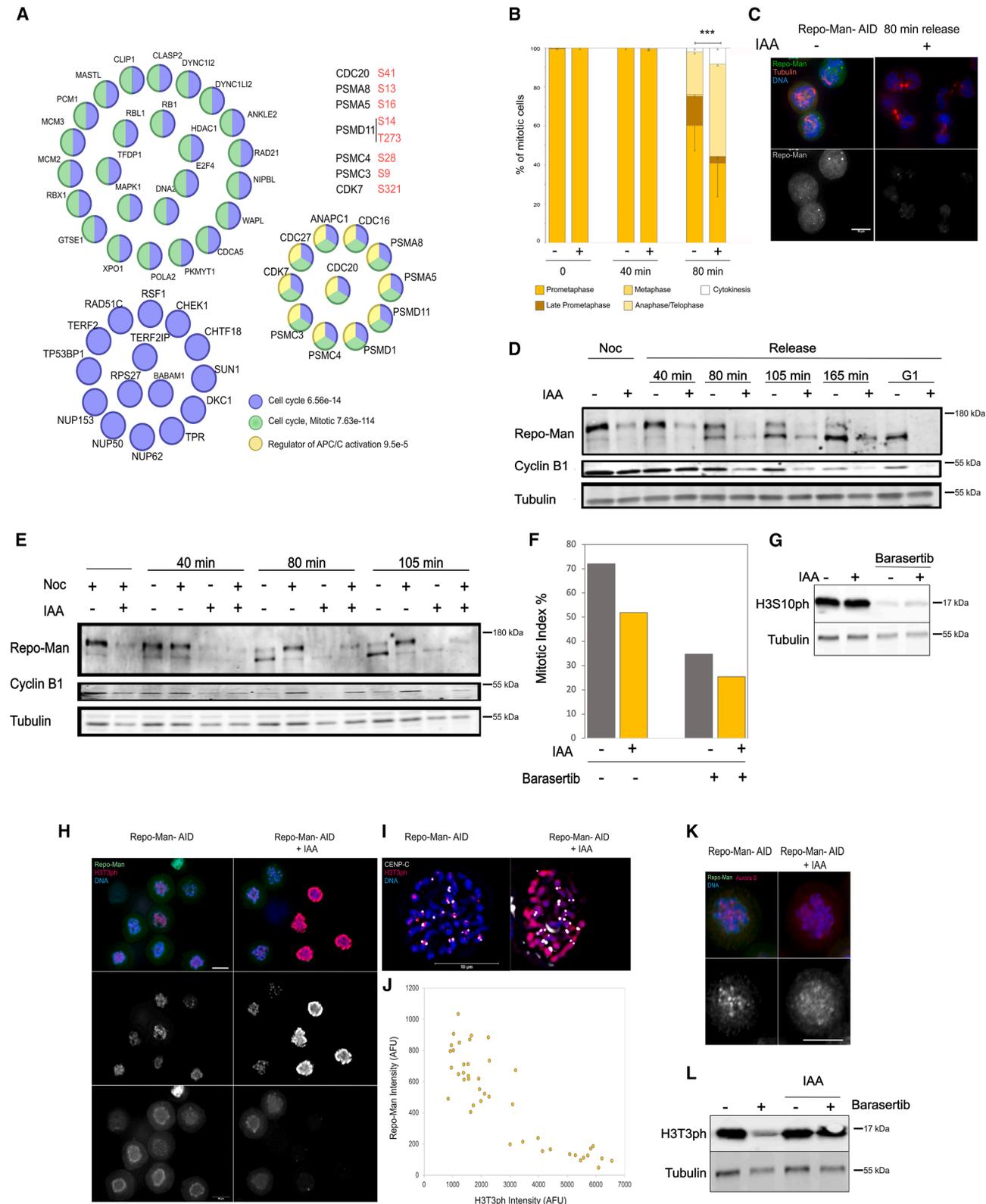
Figure 7. Repo-Man is essential for maintaining mitotic arrest

(A) String analysis of differentially phosphorylated proteins from Figure 5B for HCT116:Repo-Man-AID cell line.

(B) Quantification of mitotic stages at 0, 40, and 80 min post release from nocodazole ± IAA. Sample size: control: 0 = 194, 40 = 208, and 80 = 199; IAA: 0 = 200, 40 = 203, and 80 = 165. n = 2 biological replicates. Chi-squared test: ***$p < 0.0001$.

the cells with Repo-Man are in prometaphase/metaphase, whereas 50% of the cells without Repo-Man have progressed to anaphase/telophase (Figures 7B and 7C). In agreement with this, cyclin B is degraded at a faster rate in cells without Repo-Man (Figure 7D). In nocodazole-blocked cells, where the checkpoint is very strong, Repo-Man degradation also leads to cyclin B decrease and mitotic index (Figures 7E and 7F, left bars). These data clearly indicate that Repo-Man is necessary for maintaining cells in mitosis. We and others have shown that Repo-Man depletion by RNAi causes H3T3ph mis-localization in mitosis and suggested this phosphosite as a substrate.[11,12] However, the experiments could not discriminate between a function of the complex at mitotic entry and a requirement for Repo-Man throughout mitosis. We tested this by degrading Repo-Man while cells were already in mitosis, and we observed increased H3T3ph levels as well as its spreading along the chromosome arms (Figures 7H and 7I). This agrees with previous results and shows that the Repo-Man/PP1 complex is active in mitosis and continuously counteracts the haspin kinase. We also show a correlation between Repo-Man and H3T3ph levels (Figure 7J) and, as expected, impaired Aurora B localization (Figure 7K).

We then considered whether the effect of Repo-Man depletion in mitosis is solely mediated by Aurora B. We tested this by analyzing the mitotic index of nocodazole-arrested cells, followed by degradation of Repo-Man and inhibition of Aurora B by the highly selective inhibitor barasetib;[73] an experiment impossible to conduct without the Repo-Man degron cell line; the hypothesis was that, if Repo-Man works on the same pathway as Aurora B, inhibition of Aurora B in the presence or absence of Repo-Man would have the same effect. However, this was not the case because degradation of Repo-Man has an additive effect on Aurora B inhibition (Figure 7F), suggesting that Repo-Man might also affect another pathway. However, we cannot rule out that the phenotype represents the sum of inhibition and delocalization of an already impaired Aurora B that could further aggravate the mitotic phenotype. The efficient inhibition of Aurora B was also monitored by analyzing the level of its known mitotic substrate H3S10ph (an Aurora B substrate) (Figure 7G). In these experimental conditions, we also saw a decrease in H3T3ph upon Aurora B inhibition, as previously reported, and interpreted as the result of haspin kinase inhibition, which requires Aurora B for its activity.[74] Surprisingly, we did see a rescue of H3T3 phosphorylation levels when we degraded Repo-Man and inhibited Aurora B (Figure 7L). These results seem to indicate that haspin activity toward H3T3 phosphorylation does not depend on Aurora B and that the effect of Aurora B

inhibition on H3T3 levels (decreased) is principally mediated by the re-localization of Repo-Man to the chromatin.[72]

Altogether, this unbiased approach has revealed an essential role for Repo-Man in maintaining the mitotic checkpoint, and future work will unveil how this Repo-Man function intersects with the spindle assembly checkpoint (SAC) regulation.

DISCUSSION

The identification of protein-specific roles and contributions to cell-cycle progression has been hindered by the limitation of methodologies that are not sufficiently targeted to a particular cell-cycle transition. Degradation tags leading to rapid protein depletion have allowed us to revisit some of these aspects. Many important studies have been hypothesis driven, but they have also limited the discovery of unknown and unpredicted mechanisms. By combining a rapid protein degradation approach with unbiased multi-omics, we investigated the role of three chromatin-associated PP1-targeting subunits in mitotic exit progression and G1 nuclear program establishment. Protein degradation was conducted when cells were already in prometaphase (thus eliminating effects linked to S phase, DNA damage repair, and mitotic entry) and then allowed to progress through mitotic exit. We followed three key mitotic exit events: (1) transcription resumption, (2) chromatin accessibility, and (3) protein dephosphorylation. This unbiased approach, besides providing the community with important datasets, led us to unveil specific functions of these RIPPOs in mitotic exit.

We showed that there is no redundancy in the system, and each protein has a very specific profile, even if some sequence similarities and phylogeny might have hypothesized that Ki-67 and Repo-Man could potentially complement each other.[8]

We have also demonstrated that these RIPPOs are essential for a faithful mitotic exit and G1 re-establishment, and lack of each one leads to a G1 block. We revealed that, for Ki-67 and Repo-Man, chromosome mis-segregation is the cause of the block. However, the mechanisms differ: lack of Repo-Man caused premature mitotic exit and attenuation of the SAC, but lack of Ki-67 led to defects in the centromere chromatin structure. We could rule out a prominent role of PNUTS in maintaining or exiting mitosis, as was previously suggested,[49] and we did not observe changes in chromatin de-condensation in this *in vivo* system, making it unlikely that PNUTS plays a key role in chromatin de-condensation.[21]

We identified PNUTS as a major player in regulating transcription at this cell-cycle transition. Molecularly, we showed increased nuclear levels of RNA Pol II S5ph already in G1,

(C) Representative images of HCT116:Repo-Man-AID cells at 80 min post release from nocodazole, ± IAA, immunostained for α-tubulin. Scale bar, 10 μm.

(D) HCT116:Repo-Man-AID cells (as in Figure 1A) were collected at 40, 80, 105, and 165 min or overnight after the release from nocodazole, ± IAA. Whole-cell lysates (WCLs) were blotted for Repo-Man, anti-cyclin B1, and anti-α-tubulin (bottom).

(E) HCT116:Repo-Man-AID cells (as in Figure 1A) or kept in nocodazole. Cells were collected at 40, 80, or 105 min after release from nocodazole, ± IAA. WCLs were blotted for Repo-Man, cyclin B1, and α-tubulin.

(F) Mitotic index quantification of HCT116:Repo-Man-AID cells arrested in nocodazole (18 h), then ± IAA for 4 h, with or without barasertib. $n = 2$ biological replicates.

(G) Western blot analysis of HCT116:Repo-Man-AID cells treated as in (F). WCLs were blotted for H3S10ph and α-tubulin.

(H and I) Representative images of H3T3ph immunostaining alone (H) or with CENP-C (I) of HCT116:Repo-Man-AID cells treated as in (F).

(J) Quantification of the experiment in (I), R2 = 0.756.

(K) Representative images of Aurora B immunostaining of HCT116:Repo-Man-AID cells treated as in (F). Scale bar, 10 μm.

(L) Western blot of WCL of HCT116:Repo-Man-AID cells treated as in (F). The blots were probed for H3S10ph and tubulin.

Developmental Cell
Resource

CellPress
OPEN ACCESS

whereas it was previously reported during replication upon PNUTS knockdown.

Mitotic exit without each of the proteins triggered an interferon response; this was expected for Repo-Man and Ki-67 due to aneuploidy, but PNUTS-lacking cells are not aneuploid. By comparing the two responses, we distinguished an interferon signature for the aneuploidy-induced response and a transcription-misregulation-linked one. Genes such as IFITM1, OAS2, PSMB8, MX1, ITGB3, and IRF7 are common to both systems, but IFIT1B, IFIT3, RIOK3, CFB, DHX58, HLA-C, CDC274, CLU, LILRB1, PSMB9, and GAB2 are only shared between Repo-Man and Ki-67. It will be interesting to evaluate these gene signatures in situations of chronic aneuploidy, such as Down syndrome, but also to understand their role in chromosome instability (CIN)-driven cancers.

The differential phosphoproteomics also gave us clues on how to interpret such datasets. First, we observed several differentially hyperphosphorylated proteins when cells exited mitosis in the absence of each protein; however, comparisons with the differential prometaphase phosphoproteomes revealed a high percentage of common proteins. This suggests that caution should be exerted when analyzing these types of datasets; in fact, the G1 phosphoproteome does not only represent bona fide mitotic exit targets but also includes legacies from mitosis. Omitting this distinction could lead to very different interpretations and should be considered in future investigations.

Phosphoproteomic analyses in mitosis also provided us with unexpected clues on Repo-Man and Ki-67 mitotic functions. We showed that Repo-Man is active in M phase and essential for maintaining SAC signaling, and the premature mitotic exit observed without Repo-Man seems not to be solely mediated by Aurora B. We also discovered APC/C phospho-sites whose dephosphorylation is linked to APC/C activation; however, their role in APC/C activity regulation remains to be formally demonstrated.

This unbiased approach provided a clear link between Ki-67 and centromeric maintenance. Several centromeric proteins, including CENP-C, change phosphorylation status upon Ki-67 degradation in prometaphase. Phosphorylation of CENP-C by Aurora B has been shown to facilitate kinetochore attachment-error correction in mitosis,[75] but CDK1-mediated CENP-C phosphorylation also seems to modulate CENP-A binding and mitotic kinetochore localization:[76] these changes alone could explain the aneuploidy observed upon Ki-67 degradation. We and others reported defects in centromeric chromatin replication and structure upon Ki-67 degradation during S phase,[18,77] and previous observations reported Ki-67 co-localization with satellite DNA in G1.[25] Here, we show that Ki-67 is indeed in proximity to the centromere in mitosis, and its degradation affects centromeric compaction as well as CENP-B and CENP-C localization. These findings are interesting in several respects. RNAi depletion of chromosome periphery proteins recruited by Ki-67 has been linked to chromosome segregation defects,[60,78–81] but Ki-67 null cells did not present segregation defects;[71] here, we show that cells acutely depleted of Ki-67 do show mis-segregation defects. Interestingly, Ki-67 has been suggested as the homolog in metazoans of "bridging," a kinetochore component identified in *Cryptococcus neoformans* that connects the outer kinetochore to centromeric chromatin,[82] but no reports have associated Ki-67 with kinetochores in higher eukaryotes. Our findings show that this seems to be the case. It would be interesting to understand how these two related proteins work together to maintain a functional kinetochore across species.

Limitations of the study

The datasets and analyses derive from one cell type and may differ in other cells.

The datasets were obtained from chemically synchronized populations; this may affect the amplitude and nature of the response.

RESOURCE AVAILABILITY

Lead contact

Requests for further information and resources should be directed to and will be fulfilled by the lead contact, Paola Vagnarelli (paola.vagnarelli@brunel.ac.uk).

Materials availability

All unique/stable reagents generated in this study are available from the lead contact with a completed materials transfer agreement.

Data and code availability

- ATAC-seq, RNA-seq, and ChIP-seq data have been deposited at ArrayExpress as E-MTAB-13826, E-MTAB-13827, and E-MTAB-15533 and are publicly available as of the date of publication. Mass spectrometry data have been deposited at PRIDE as PXD049319 and are publicly available as of the date of publication.
- This paper analyzes existing, publicly available data, accessible at GEO: GSE186206 (Ki-67), GEO: GSE54170 (Repo-Man and PNUTS), GEO: GSE84035 (*in vitro* binding sequencing data for Repo-Man), GEO: GSM8413578 (PNUTS ChIP dataset), GEO: GSE86667 (H3K9me3), and GEO: GSM5640483 (LMNB1).
- This paper does not report original code.
- Any additional information required to reanalyze the data reported in this paper is available from the lead contact upon request.

AUTHOR CONTRIBUTIONS

Conceptualization, P.V. and C.S.; methodology, K.S., F.H., M.B., C.S., J.R., and P.V.; formal analysis, K.S., F.H., M.B., D.R., I.J.d.C., C.S., and P.V.; investigation, K.S., F.H., M.B., D.R., I.J.d.C., C.S., and P.V.; data curation, K.S., F.H., M.B., C.S., J.R., and P.V.; writing – review and editing, P.V., with contributions from all authors; visualization, P.V., K.S., F.H., and M.B.; supervision, P.V., C.S., and J.R.; funding acquisition, P.V.

DECLARATION OF INTERESTS

The authors declare no competing interests.

STAR★METHODS

Detailed methods are provided in the online version of this paper and include the following:

- KEY RESOURCES TABLE
- EXPERIMENTAL MODEL AND STUDY PARTICIPANT DETAILS
  - Cell lines
- METHOD DETAILS
  - Plasmids
  - Cell line generation
  - Mitotic synchronisation and protein degradation for G1 analyses
  - Immunofluorescence microscopy
  - Immunoblotting
  - CDK2 activity analyses
  - APC/C activity analyses
  - Comet assay
  - Fluorescence in situ hybridisation (FISH)
  - Pericentromeric/α-satellite FISH
  - Proximity ligation assay (PLA)
  - RNA sequencing
  - ATAC sequencing
  - Pearson correlation
  - Mass spectrometry
  - Chromatin immunoprecipitation (ChIP)
  - ChIP-seq analysis
  - Co-occupancy analysis
  - Analysis of publicly available datasets
- QUANTIFICATION AND STATISTICAL ANALYSES
  - FISH analyses
  - CENP-B
  - PLA
  - Nuclear area
  - RNA Polymerase II (POL II)
  - Statistical analyses

SUPPLEMENTAL INFORMATION

Supplemental information can be found online at https://doi.org/10.1016/j.devcel.2026.02.016.

REFERENCES

1. Abramo, K., Valton, A.L., Venev, S.V., Ozadam, H., Fox, A.N., and Dekker, J. (2019). A chromosome folding intermediate at the condensin-to-cohesin transition during telophase. Nat. Cell Biol. 21, 1393–1402. https://doi.org/10.1038/s41556-019-0406-2.

2. Hildebrand, E.M., Polovnikov, K., Dekker, B., Liu, Y., Lafontaine, D.L., Fox, A.N., Li, Y., Venev, S.V., Mirny, L.A., and Dekker, J. (2024). Mitotic chromosomes are self-entangled and disentangle through a topoisomerase-II-dependent two-stage exit from mitosis. Mol. Cell 84, 1422–1441.e14. https://doi.org/10.1016/j.molcel.2024.02.025.

3. Solovei, I., Wang, A.S., Thanisch, K., Schmidt, C.S., Krebs, S., Zwerger, M., Cohen, T.V., Devys, D., Foisner, R., Peichl, L., et al. (2013). LBR and lamin A/C sequentially tether peripheral heterochromatin and inversely regulate differentiation. Cell 152, 584–598. https://doi.org/10.1016/j.cell.2013.01.009.

4. Wong, X., Hoskins, V.E., Melendez-Perez, A.J., Harr, J.C., Gordon, M., and Reddy, K.L. (2021). Lamin C is required to establish genome organization after mitosis. Genome Biol. 22, 305. https://doi.org/10.1186/s13059-021-02516-7.

5. Palozola, K.C., Donahue, G., Liu, H., Grant, G.R., Becker, J.S., Cote, A., Yu, H., Raj, A., and Zaret, K.S. (2017). Mitotic transcription and waves of gene reactivation during mitotic exit. Science 358, 119–122. https://doi.org/10.1126/science.aal4671.

6. Cundell, M.J., Hutter, L.H., Nunes Bastos, R., Poser, E., Holder, J., Mohammed, S., Novak, B., and Barr, F.A. (2016). A PP2A-B55 recognition signal controls substrate dephosphorylation kinetics during mitotic exit. J. Cell Biol. 214, 539–554. https://doi.org/10.1083/jcb.201606033.

7. Trinkle-Mulcahy, L., Andersen, J., Lam, Y.W., Moorhead, G., Mann, M., and Lamond, A.I. (2006). Repo-Man recruits PP1 gamma to chromatin and is essential for cell viability. J. Cell Biol. 172, 679–692. https://doi.org/10.1083/jcb.200508154.

8. Booth, D.G., Takagi, M., Sanchez-Pulido, L., Petfalski, E., Vargiu, G., Samejima, K., Imamoto, N., Ponting, C.P., Tollervey, D., Earnshaw, W.C., et al. (2014). Ki-67 is a PP1-interacting protein that organises the mitotic chromosome periphery. eLife 3, e01641. https://doi.org/10.7554/eLife.01641.

9. Allen, P.B., Kwon, Y.G., Nairn, A.C., and Greengard, P. (1998). Isolation and characterization of PNUTS, a putative protein phosphatase 1 nuclear targeting subunit. J. Biol. Chem. 273, 4089–4095. https://doi.org/10.1074/jbc.273.7.4089.

10. Kreivi, J.P., Trinkle-Mulcahy, L., Lyon, C.E., Morrice, N.A., Cohen, P., and Lamond, A.I. (1997). Purification and characterisation of p99, a nuclear modulator of protein phosphatase 1 activity. FEBS Lett. 420, 57–62. https://doi.org/10.1016/s0014-5793(97)01485-3.

11. Qian, J., Lesage, B., Beullens, M., Van Eynde, A., and Bollen, M. (2011). PP1/Repo-man dephosphorylates mitotic histone H3 at T3 and regulates chromosomal aurora B targeting. Curr. Biol. 21, 766–773. https://doi.org/10.1016/j.cub.2011.03.047.

12. Vagnarelli, P., Ribeiro, S., Sennels, L., Sanchez-Pulido, L., de Lima Alves, F., Verheyen, T., Kelly, D.A., Ponting, C.P., Rappsilber, J., and Earnshaw, W.C. (2011). Repo-Man coordinates chromosomal reorganization with nuclear envelope reassembly during mitotic exit. Dev. Cell 21, 328–342. https://doi.org/10.1016/j.devcel.2011.06.020.

13. de Castro, I.J., Budzak, J., Di Giacinto, M.L., Ligammari, L., Gokhan, E., Spanos, C., Moralli, D., Richardson, C., de Las Heras, J.I., Salatino, S., et al. (2017). Repo-Man/PP1 regulates heterochromatin formation in interphase. Nat. Commun. 8, 14048. https://doi.org/10.1038/ncomms14048.

14. Huguet, F., Gokan, E., Foster, H.A., Amin, H.A., and Vagnarelli, P. (2022). Repo-Man/protein phosphatase 1 SUMOylation mediates binding to lamin A and serine 22 dephosphorylation. Open Biol. 12, 220017. https://doi.org/10.1098/rsob.220017.

15. Moriuchi, T., and Hirose, F. (2021). SUMOylation of RepoMan during late telophase regulates dephosphorylation of lamin A. J. Cell Sci. 134, jcs247171. https://doi.org/10.1242/jcs.247171.

16. Sobecki, M., Mrouj, K., Camasses, A., Parisis, N., Nicolas, E., Llères, D., Gerbe, F., Prieto, S., Krasinska, L., David, A., et al. (2016). The cell proliferation antigen Ki-67 organises heterochromatin. eLife 5, e13722. https://doi.org/10.7554/eLife.13722.

17. Sun, X., Bizhanova, A., Matheson, T.D., Yu, J., Zhu, L.J., and Kaufman, P.D. (2017). Ki-67 Contributes to Normal Cell Cycle Progression and Inactive X Heterochromatin in p21 Checkpoint-Proficient Human Cells. Mol. Cell. Biol. 37, e00569-16. https://doi.org/10.1128/MCB.00569-16.

18. van Schaik, T., Manzo, S.G., Vouzas, A.E., Liu, N.Q., Teunissen, H., de Wit, E., Gilbert, D.M., and van Steensel, B. (2022). Dynamic chromosomal interactions and control of heterochromatin positioning by Ki-67. EMBO Rep. 23, e55782. https://doi.org/10.15252/embr.202255782.

19. Landsverk, H.B., Sandquist, L.E., Bay, L.T.E., Steurer, B., Campsteijn, C., Landsverk, O.J.B., Marteijn, J.A., Petermann, E., Trinkle-Mulcahy, L., and Syljuåsen, R.G. (2020). WDR82/PNUTS-PP1 Prevents Transcription-Replication Conflicts by Promoting RNA Polymerase II Degradation on Chromatin. Cell Rep. 33, 108469. https://doi.org/10.1016/j.celrep.2020.108469.

20. Estell, C., Davidson, L., Eaton, J.D., Kimura, H., Gold, V.A.M., and West, S. (2023). A restrictor complex of ZC3H4, WDR82, and ARS2 integrates with

PNUTS to control unproductive transcription. Mol. Cell 83, 2222–2239.e5. https://doi.org/10.1016/j.molcel.2023.05.029.

21. Landsverk, H.B., Kirkhus, M., Bollen, M., Küntziger, T., and Collas, P. (2005). PNUTS enhances in vitro chromosome decondensation in a PP1-dependent manner. Biochem. J. 390, 709–717. https://doi.org/10.1042/BJ20050678.

22. Udho, E., Tedesco, V.C., Zygmunt, A., and Krucher, N.A. (2002). PNUTS (phosphatase nuclear targeting subunit) inhibits retinoblastoma-directed PP1 activity. Biochem. Biophys. Res. Commun. 297, 463–467. https://doi.org/10.1016/s0006-291x(02)02236-2.

23. Krucher, N.A., Rubin, E., Tedesco, V.C., Roberts, M.H., Sherry, T.C., and De Leon, G. (2006). Dephosphorylation of Rb (Thr-821) in response to cell stress. Exp. Cell Res. 312, 2757–2763. https://doi.org/10.1016/j.yexcr.2006.05.002.

24. Kavela, S., Shinde, S.R., Ratheesh, R., Viswakalyan, K., Bashyam, M.D., Gowrishankar, S., Vamsy, M., Pattnaik, S., Rao, S., Sastry, R.A., et al. (2013). PNUTS functions as a proto-oncogene by sequestering PTEN. Cancer Res. 73, 205–214. https://doi.org/10.1158/0008-5472.CAN-12-1394.

25. Bridger, J.M., Kill, I.R., and Lichter, P. (1998). Association of pKi-67 with satellite DNA of the human genome in early G1 cells. Chromosome Res. 6, 13–24. https://doi.org/10.1023/a:1009210206855.

26. Stamatiou, K., Huguet, F., Serapinas, L.V., Spanos, C., Rappsilber, J., and Vagnarelli, P. (2024). Ki-67 is necessary during DNA replication for fork protection and genome stability. Genome Biol. 25, 105. https://doi.org/10.1186/s13059-024-03243-5.

27. Verheyen, T., Görnemann, J., Verbinnen, I., Boens, S., Beullens, M., Van Eynde, A., and Bollen, M. (2015). Genome-wide promoter binding profiling of protein phosphatase-1 and its major nuclear targeting subunits. Nucleic Acids Res. 43, 5771–5784. https://doi.org/10.1093/nar/gkv500.

28. Bejjani, F., Ségéral, E., Mosca, K., Lecourieux, A., Bakail, M., Hamoudi, M., and Emiliani, S. (2025). Overlapping and distinct functions of SPT6, PNUTS, and PCF11 in regulating transcription termination. Nucleic Acids Res. 53, gkaf179. https://doi.org/10.1093/nar/gkaf179.

29. Holder, J., Mohammed, S., and Barr, F.A. (2020). Ordered dephosphorylation initiated by the selective proteolysis of cyclin B drives mitotic exit. eLife 9, e59885. https://doi.org/10.7554/eLife.59885.

30. Cuylen-Haering, S., Petrovic, M., Hernandez-Armendariz, A., Schneider, M.W.G., Samwer, M., Blaukopf, C., Holt, L.J., and Gerlich, D.W. (2020). Chromosome clustering by Ki-67 excludes cytoplasm during nuclear assembly. Nature 587, 285–290. https://doi.org/10.1038/s41586-020-2672-3.

31. Spencer, S.L., Cappell, S.D., Tsai, F.C., Overton, K.W., Wang, C.L., and Meyer, T. (2013). The proliferation-quiescence decision is controlled by a bifurcation in CDK2 activity at mitotic exit. Cell 155, 369–383. https://doi.org/10.1016/j.cell.2013.08.062.

32. Fischer, M., Schade, A.E., Branigan, T.B., Müller, G.A., and DeCaprio, J.A. (2022). Coordinating gene expression during the cell cycle. Trends Biochem. Sci. 47, 1009–1022. https://doi.org/10.1016/j.tibs.2022.06.007.

33. Zhang, S., Valenzuela, L.F., Zatulovskiy, E., Mangiante, L., Curtis, C., and Skotheim, J.M. (2024). The G1/S transition is promoted by Rb degradation via the E3 ligase UBR5. Preprint at bioRxiv. https://doi.org/10.1101/2023.10.03.560768.

34. De Leon, G., Sherry, T.C., and Krucher, N.A. (2008). Reduced expression of PNUTS leads to activation of Rb-phosphatase and caspase-mediated apoptosis. Cancer Biol. Ther. 7, 833–841. https://doi.org/10.4161/cbt.7.6.5839.

35. Choy, M.S., Hieke, M., Kumar, G.S., Lewis, G.R., Gonzalez-DeWhitt, K.R., Kessler, R.P., Stein, B.J., Hessenberger, M., Nairn, A.C., Peti, W., et al. (2014). Understanding the antagonism of retinoblastoma protein dephosphorylation by PNUTS provides insights into the PP1 regulatory code. Proc. Natl. Acad. Sci. USA 111, 4097–4102. https://doi.org/10.1073/pnas.1317395111.

36. Konagaya, Y., Rosenthal, D., Ratnayeke, N., Fan, Y., and Meyer, T. (2024). An intermediate Rb-E2F activity state safeguards proliferation commitment. Nature 631, 424–431. https://doi.org/10.1038/s41586-024-07554-2.

37. Mackenzie, K.J., Carroll, P., Martin, C.A., Murina, O., Fluteau, A., Simpson, D.J., Olova, N., Sutcliffe, H., Rainger, J.K., Leitch, A., et al. (2017). cGAS surveillance of micronuclei links genome instability to innate immunity. Nature 548, 461–465. https://doi.org/10.1038/nature23449.

38. Bigot, N., Day, M., Baldock, R.A., Watts, F.Z., Oliver, A.W., and Pearl, L.H. (2019). Phosphorylation-mediated interactions with TOPBP1 couple 53BP1 and 9-1-1 to control the G1 DNA damage checkpoint. eLife 8, e44353. https://doi.org/10.7554/eLife.44353.

39. Cantres-Velez, J.A., Blaize, J.L., Vierra, D.A., Boisvert, R.A., Garzon, J.L., Piraino, B., Tan, W., Deans, A.J., and Howlett, N.G. (2021). Cyclin-Dependent Kinase-Mediated Phosphorylation of FANCD2 Promotes Mitotic Fidelity. Mol. Cell. Biol. 41, e0023421. https://doi.org/10.1128/MCB.00234-21.

40. Anamika, and Spyracopoulos, L. (2016). Molecular Basis for Phosphorylation-dependent SUMO Recognition by the DNA Repair Protein RAP80. J. Biol. Chem. 291, 4417–4428. https://doi.org/10.1074/jbc.M115.705061.

41. Yan, J., Yang, X.P., Kim, Y.S., and Jetten, A.M. (2008). RAP80 responds to DNA damage induced by both ionizing radiation and UV irradiation and is phosphorylated at Ser 205. Cancer Res. 68, 4269–4276. https://doi.org/10.1158/0008-5472.CAN-07-5950.

42. Hervé, S., Scelfo, A., Bersano Marchisio, G., Grison, M., Vaidžiulytė, K., Dumont, M., Angrisani, A., Keikhosravi, A., Pegoraro, G., Deygas, M., et al. (2025). Chromosome mis-segregation triggers cell cycle arrest through a mechanosensitive nuclear envelope checkpoint. Nat. Cell Biol. 27, 73–86. https://doi.org/10.1038/s41556-024-01565-x.

43. Mrouj, K., Andrés-Sánchez, N., Dubra, G., Singh, P., Sobecki, M., Chahar, D., Al Ghoul, E., Aznar, A.B., Prieto, S., Pirot, N., et al. (2021). Ki-67 regulates global gene expression and promotes sequential stages of carcinogenesis. Proc. Natl. Acad. Sci. USA 118, e2026507118. https://doi.org/10.1073/pnas.2026507118.

44. Zheng, J.N., Pei, D.S., Mao, L.J., Liu, X.Y., Mei, D.D., Zhang, B.F., Shi, Z., Wen, R.M., and Sun, X.Q. (2009). Inhibition of renal cancer cell growth in vitro and in vivo with oncolytic adenovirus armed short hairpin RNA targeting Ki-67 encoding mRNA. Cancer Gene Ther. 16, 20–32. https://doi.org/10.1038/cgt.2008.61.

45. Kausch, I., Jiang, H., Brocks, C., Bruderek, K., Krüger, S., Sczakiel, G., Jocham, D., and Böhle, A. (2004). Ki-67-directed antisense therapy in an orthotopic renal cell carcinoma model. discussion 124. Eur. Urol. 46, 118–124. https://doi.org/10.1016/j.eururo.2004.03.016.

46. Kausch, I., Jiang, H., Ewerdwalbesloh, N., Doehn, C., Krüger, S., Sczakiel, G., and Jocham, D. (2005). Inhibition of Ki-67 in a renal cell carcinoma severe combined immunodeficiency disease mouse model is associated with induction of apoptosis and tumour growth inhibition. BJU Int. 95, 416–420. https://doi.org/10.1111/j.1464-410X.2005.05312.x.

47. Ciurciu, A., Duncalf, L., Jonchere, V., Lansdale, N., Vasieva, O., Glenday, P., Rudenko, A., Vissi, E., Cobbe, N., Alphey, L., et al. (2013). PNUTS/PP1 regulates RNAPII-mediated gene expression and is necessary for developmental growth. PLoS Genet. 9, e1003885. https://doi.org/10.1371/journal.pgen.1003885.

48. Cortazar, M.A., Sheridan, R.M., Erickson, B., Fong, N., Glover-Cutter, K., Brannan, K., and Bentley, D.L. (2019). Control of RNA Pol II Speed by PNUTS-PP1 and Spt5 Dephosphorylation Facilitates Termination by a "Sitting Duck Torpedo" Mechanism. Mol. Cell 76, 896–908.e4. https://doi.org/10.1016/j.molcel.2019.09.031.

49. Wang, F., Wang, L., Fisher, L.A., Li, C., Wang, W., and Peng, A. (2019). Phosphatase 1 Nuclear Targeting Subunit (PNUTS) Regulates Aurora Kinases and Mitotic Progression. Mol. Cancer Res. 17, 10–19. https://doi.org/10.1158/1541-7786.MCR-17-0670.

CellPress
OPEN ACCESS

Developmental Cell
Resource

50. Lee, J.H., You, J., Dobrota, E., and Skalnik, D.G. (2010). Identification and characterization of a novel human PP1 phosphatase complex. J. Biol. Chem. *285*, 24466–24476. https://doi.org/10.1074/jbc.M110.109801.

51. Hatchi, E., Skourti-Stathaki, K., Ventz, S., Pinello, L., Yen, A., Kamieniarz-Gdula, K., Dimitrov, S., Pathania, S., McKinney, K.M., Eaton, M.L., et al. (2015). BRCA1 recruitment to transcriptional pause sites is required for R-loop-driven DNA damage repair. Mol. Cell *57*, 636–647. https://doi.org/10.1016/j.molcel.2015.01.011.

52. Morales, J.C., Richard, P., Patidar, P.L., Motea, E.A., Dang, T.T., Manley, J.L., and Boothman, D.A. (2016). XRN2 Links Transcription Termination to DNA Damage and Replication Stress. PLoS Genet. *12*, e1006107. https://doi.org/10.1371/journal.pgen.1006107.

53. Skourti-Stathaki, K., Proudfoot, N.J., and Gromak, N. (2011). Human senataxin resolves RNA/DNA hybrids formed at transcriptional pause sites to promote Xrn2-dependent termination. Mol. Cell *42*, 794–805. https://doi.org/10.1016/j.molcel.2011.04.026.

54. Bou-Nader, C., Bothra, A., Garboczi, D.N., Leppla, S.H., and Zhang, J. (2022). Structural basis of R-loop recognition by the S9.6 monoclonal antibody. Nat. Commun. *13*, 1641. https://doi.org/10.1038/s41467-022-29187-7.

55. Vagnarelli, P. (2021). Back to the new beginning: Mitotic exit in space and time. Semin. Cell Dev. Biol. *117*, 140–148. https://doi.org/10.1016/j.semcdb.2021.03.010.

56. Kumar, G.S., Gokhan, E., De Munter, S., Bollen, M., Vagnarelli, P., Peti, W., and Page, R. (2016). The Ki-67 and RepoMan mitotic phosphatases assemble via an identical, yet novel mechanism. eLife *5*, e16539. https://doi.org/10.7554/eLife.16539.

57. Takagi, M., Nishiyama, Y., Taguchi, A., and Imamoto, N. (2014). Ki67 antigen contributes to the timely accumulation of protein phosphatase 1gamma on anaphase chromosomes. J. Biol. Chem. *289*, 22877–22887. https://doi.org/10.1074/jbc.M114.556647.

58. De Munter, S., Görnemann, J., Derua, R., Lesage, B., Qian, J., Heroes, E., Waelkens, E., Van Eynde, A., Beullens, M., and Bollen, M. (2017). Split-BioID: a proximity biotinylation assay for dimerization-dependent protein interactions. FEBS Lett. *591*, 415–424. https://doi.org/10.1002/1873-3468.12548.

59. Kommer, D.C., Stamatiou, K., and Vagnarelli, P. (2024). Cell Cycle-Specific Protein Phosphatase 1 (PP1) Substrates Identification Using Genetically Modified Cell Lines. Methods Mol. Biol. *2740*, 37–61. https://doi.org/10.1007/978-1-0716-3557-5_3.

60. Stamatiou, K., Chmielewska, A., Ohta, S., Earnshaw, W.C., and Vagnarelli, P. (2023). CCDC86 is a novel Ki-67-interacting protein important for cell division. J. Cell Sci. *136*, jcs260391. https://doi.org/10.1242/jcs.260391.

61. Kabella, N., Bayer, F.P., Stamatiou, K., Abele, M., Sakhteman, A., Chang, Y.C., Wagner, V., Gabriel, A., Krumm, J., Reinecke, M., et al. (2025). Proteomic analyses identify targets, pathways, and cellular consequences of oncogenic KRAS signaling. Sci. Signal. *18*, eadt6552. https://doi.org/10.1126/scisignal.adt6552.

62. Kochin, V., Shimi, T., Torvaldson, E., Adam, S.A., Goldman, A., Pack, C.G., Melo-Cardenas, J., Imanishi, S.Y., Goldman, R.D., and Eriksson, J.E. (2014). Interphase phosphorylation of lamin A. J. Cell Sci. *127*, 2683–2696. https://doi.org/10.1242/jcs.141820.

63. Makarov, A.A., Zou, J., Houston, D.R., Spanos, C., Solovyova, A.S., Cardenal-Peralta, C., Rappsilber, J., and Schirmer, E.C. (2019). Lamin A molecular compression and sliding as mechanisms behind nucleoskeleton elasticity. Nat. Commun. *10*, 3056. https://doi.org/10.1038/s41467-019-11063-6.

64. Ladurner, R., Kreidl, E., Ivanov, M.P., Ekker, H., Idarraga-Amado, M.H., Busslinger, G.A., Wutz, G., Cisneros, D.A., and Peters, J.M. (2016). Sororin actively maintains sister chromatid cohesion. EMBO J. *35*, 635–653. https://doi.org/10.15252/embj.201592532.

65. Jeyaprakash, A.A., Basquin, C., Jayachandran, U., and Conti, E. (2011). Structural basis for the recognition of phosphorylated histone h3 by the survivin subunit of the chromosomal passenger complex. Structure *19*, 1625–1634. https://doi.org/10.1016/j.str.2011.09.002.

66. Hinshaw, S.M., Quan, Y., Cai, J., Zhou, A.L., and Zhou, H. (2023). Multi-site phosphorylation of yeast Mif2/CENP-C promotes inner kinetochore assembly. Curr. Biol. *33*, 688–696.e6. https://doi.org/10.1016/j.cub.2023.01.012.

67. Chardon, F., Japaridze, A., Witt, H., Velikovsky, L., Chakraborty, C., Wilhelm, T., Dumont, M., Yang, W., Kikuti, C., Gangnard, S., et al. (2022). CENP-B-mediated DNA loops regulate activity and stability of human centromeres. Mol. Cell *82*, 1751–1767.e8. https://doi.org/10.1016/j.molcel.2022.02.032.

68. Saiwaki, T., Kotera, I., Sasaki, M., Takagi, M., and Yoneda, Y. (2005). In vivo dynamics and kinetics of pKi-67: transition from a mobile to an immobile form at the onset of anaphase. Exp. Cell Res. *308*, 123–134. https://doi.org/10.1016/j.yexcr.2005.04.010.

69. Hori, T., Shang, W.H., Toyoda, A., Misu, S., Monma, N., Ikeo, K., Molina, O., Vargiu, G., Fujiyama, A., Kimura, H., et al. (2014). Histone H4 Lys 20 monomethylation of the CENP-A nucleosome is essential for kinetochore assembly. Dev. Cell *29*, 740–749. https://doi.org/10.1016/j.devcel.2014.05.001.

70. Altemose, N., Maslan, A., Smith, O.K., Sundararajan, K., Brown, R.R., Mishra, R., Detweiler, A.M., Neff, N., Miga, K.H., Straight, A.F., et al. (2022). DiMeLo-seq: a long-read, single-molecule method for mapping protein-DNA interactions genome wide. Nat. Methods *19*, 711–723. https://doi.org/10.1038/s41592-022-01475-6.

71. Cuylen, S., Blaukopf, C., Politi, A.Z., Müller-Reichert, T., Neumann, B., Poser, I., Ellenberg, J., Hyman, A.A., and Gerlich, D.W. (2016). Ki-67 acts as a biological surfactant to disperse mitotic chromosomes. Nature *535*, 308–312. https://doi.org/10.1038/nature18610.

72. Qian, J., Beullens, M., Lesage, B., and Bollen, M. (2013). Aurora B defines its own chromosomal targeting by opposing the recruitment of the phosphatase scaffold Repo-Man. Curr. Biol. *23*, 1136–1143. https://doi.org/10.1016/j.cub.2013.05.017.

73. Johnson, M.L., Wang, J.S., Falchook, G., Greenlees, C., Jones, S., Strickland, D., Fabbri, G., Kennedy, C., Elizabeth Pease, J., Sainsbury, L., et al. (2023). Safety, tolerability, and pharmacokinetics of Aurora kinase B inhibitor AZD2811: a phase 1 dose-finding study in patients with advanced solid tumours. Br. J. Cancer *128*, 1906–1915. https://doi.org/10.1038/s41416-023-02185-2.

74. Wang, F., Ulyanova, N.P., van der Waal, M.S., Patnaik, D., Lens, S.M.A., and Higgins, J.M.G. (2011). A positive feedback loop involving Haspin and Aurora B promotes CPC accumulation at centromeres in mitosis. Curr. Biol. *21*, 1061–1069. https://doi.org/10.1016/j.cub.2011.05.016.

75. Zhou, X., Zheng, F., Wang, C., Wu, M., Zhang, X., Wang, Q., Yao, X., Fu, C., Zhang, X., and Zang, J. (2017). Phosphorylation of CENP-C by Aurora B facilitates kinetochore attachment error correction in mitosis. Proc. Natl. Acad. Sci. USA *114*, E10667–E10676. https://doi.org/10.1073/pnas.1710506114.

76. Watanabe, R., Hara, M., Okumura, E.I., Hervé, S., Fachinetti, D., Ariyoshi, M., and Fukagawa, T. (2019). CDK1-mediated CENP-C phosphorylation modulates CENP-A binding and mitotic kinetochore localization. J. Cell Biol. *218*, 4042–4062. https://doi.org/10.1083/jcb.201907006.

77. Stamatiou, K.H., Huguet, F., Spanos, C., Rappsilber, J., and Vagnarelli, P. (2023). Ki-67 is necessary during DNA replication for forks protection and genome stability. Genome Biol. *25*, 105. https://doi.org/10.1186/s13059-024-03243-5.

78. Fujimura, A., Hayashi, Y., Kato, K., Kogure, Y., Kameyama, M., Shimamoto, H., Daitoku, H., Fukamizu, A., Hirota, T., and Kimura, K. (2020). Identification of a novel nucleolar protein complex required for mitotic chromosome segregation through centromeric accumulation of Aurora B. Nucleic Acids Res. *48*, 6583–6596. https://doi.org/10.1093/nar/gkaa449.

79. Ma, N., Matsunaga, S., Takata, H., Ono-Maniwa, R., Uchiyama, S., and Fukui, K. (2007). Nucleolin functions in nucleolus formation and chromosome congression. J. Cell Sci. *120*, 2091–2105. https://doi.org/10.1242/jcs.008771.

Developmental Cell
Resource

CellPress
OPEN ACCESS

80. Amin, M.A., Matsunaga, S., Ma, N., Takata, H., Yokoyama, M., Uchiyama, S., and Fukui, K. (2007). Fibrillarin, a nucleolar protein, is required for normal nuclear morphology and cellular growth in HeLa cells. Biochem. Biophys. Res. Commun. *360*, 320–326. https://doi.org/10.1016/j.bbrc.2007.06.092.

81. Ugrinova, I., Monier, K., Ivaldi, C., Thiry, M., Storck, S., Mongelard, F., and Bouvet, P. (2007). Inactivation of nucleolin leads to nucleolar disruption, cell cycle arrest and defects in centrosome duplication. BMC Mol. Biol. *8*, 66. https://doi.org/10.1186/1471-2199-8-66.

82. Sridhar, S., Hori, T., Nakagawa, R., Fukagawa, T., and Sanyal, K. (2021). Bridgin connects the outer kinetochore to centromeric chromatin. Nat. Commun. *12*, 146. https://doi.org/10.1038/s41467-020-20161-9.

83. Ran, F.A., Hsu, P.D., Wright, J., Agarwala, V., Scott, D.A., and Zhang, F. (2013). Genome engineering using the CRISPR-Cas9 system. Nat. Protoc. *8*, 2281–2308. https://doi.org/10.1038/nprot.2013.143.

84. Natsume, T., Kiyomitsu, T., Saga, Y., and Kanemaki, M.T. (2016). Rapid Protein Depletion in Human Cells by Auxin-Inducible Degron Tagging with Short Homology Donors. Cell Rep. *15*, 210–218. https://doi.org/10.1016/j.celrep.2016.03.001.

85. Kendall, J., Liu, Q., Bakleh, A., Krasnitz, A., Nguyen, K.C.Q., Lakshmi, B., Gerald, W.L., Powers, S., and Mu, D. (2007). Oncogenic cooperation and coamplification of developmental transcription factor genes in lung cancer. Proc. Natl. Acad. Sci. USA *104*, 16663–16668. https://doi.org/10.1073/pnas.0708286104.

86. Schneider, C.A., Rasband, W.S., and Eliceiri, K.W. (2012). NIH Image to ImageJ: 25 years of image analysis. Nat. Methods *9*, 671–675. https://doi.org/10.1038/nmeth.2089.

87. Li, H., Handsaker, B., Wysoker, A., Fennell, T., Ruan, J., Homer, N., Marth, G., Abecasis, G., and Durbin, R.; 1000 Genome Project Data Processing Subgroup (2009). The Sequence Alignment/Map format and SAMtools. Bioinformatics *25*, 2078–2079. https://doi.org/10.1093/bioinformatics/btp352.

88. Anders, S., Pyl, P.T., and Huber, W. (2015). HTSeq–a Python framework to work with high-throughput sequencing data. Bioinformatics *31*, 166–169. https://doi.org/10.1093/bioinformatics/btu638.

89. Love, M.I., Huber, W., and Anders, S. (2014). Moderated estimation of fold change and dispersion for RNA-seq data with DESeq2. Genome Biol. *15*, 550. https://doi.org/10.1186/s13059-014-0550-8.

90. Cox, J., and Mann, M. (2008). MaxQuant enables high peptide identification rates, individualized p.p.b.-range mass accuracies and proteome-wide protein quantification. Nat. Biotechnol. *26*, 1367–1372. https://doi.org/10.1038/nbt.1511.

91. Cox, J., Neuhauser, N., Michalski, A., Scheltema, R.A., Olsen, J.V., and Mann, M. (2011). Andromeda: a peptide search engine integrated into the MaxQuant environment. J. Proteome Res. *10*, 1794–1805. https://doi.org/10.1021/pr101065j.

92. Ramírez, F., Ryan, D.P., Grüning, B., Bhardwaj, V., Kilpert, F., Richter, A.S., Heyne, S., Dündar, F., and Manke, T. (2016). deepTools2: a next generation web server for deep-sequencing data analysis. Nucleic Acids Res. *44*, W160–W165. https://doi.org/10.1093/nar/gkw257.

93. Quinlan, A.R., and Hall, I.M. (2010). BEDTools: a flexible suite of utilities for comparing genomic features. Bioinformatics *26*, 841–842. https://doi.org/10.1093/bioinformatics/btq033.

94. Zang, C., Wang, Y., and Peng, W. (2020). RECOGNICER: A coarse-graining approach for identifying broad domains from ChIP-seq data. Quant. Biol. *8*, 359–368. https://doi.org/10.1007/s40484-020-0225-2.

95. Tice, R.R., Agurell, E., Anderson, D., Burlinson, B., Hartmann, A., Kobayashi, H., Miyamae, Y., Rojas, E., Ryu, J.C., and Sasaki, Y.F. (2000). Single cell gel/comet assay: guidelines for in vitro and in vivo genetic toxicology testing. Environ Mol Mutagen *35*, 206–221. https://doi.org/10.1002/(sici)1098-2280(2000)35:3<206::aid-em8>3.0.co;2-j.

96. Wisniewski, J.R., Zougman, A., Nagaraj, N., and Mann, M. (2009). Universal sample preparation method for proteome analysis. Nat. Methods *6*, 359–362. https://doi.org/10.1038/nmeth.1322.

97. Rappsilber, J., Mann, M., and Ishihama, Y. (2007). Protocol for micro-purification, enrichment, pre-fractionation and storage of peptides for proteomics using StageTips. Nat. Protoc. *2*, 1896–1906. https://doi.org/10.1038/nprot.2007.261.

98. Olsen, J.V., Macek, B., Lange, O., Makarov, A., Horning, S., and Mann, M. (2007). Higher-energy C-trap dissociation for peptide modification analysis. Nat. Methods *4*, 709–712. https://doi.org/10.1038/nmeth1060.

99. Danecek, P., Bonfield, J.K., Liddle, J., Marshall, J., Ohan, V., Pollard, M.O., Whitwham, A., Keane, T., McCarthy, S.A., Davies, R.M., and Li, H. (2021). Twelve years of SAMtools and BCFtools. Gigascience. https://doi.org/10.1093/gigascience/giab008.

STAR★METHODS

KEY RESOURCES TABLE

REAGENT or RESOURCE	SOURCE	IDENTIFIER
Antibodies		
Mouse monoclonal anti-a-tubulin (clone B-5-1-2)	Sigma-Aldrich	Cat# T5168; RRID:AB_477579
Mouse monoclonal anti-GAPDH	Proteintech	Cat# 60004-1-Ig, RRID:AB_2107436
Rabbit polyclonal anti-GFP [PABG1]	Chromotek	Cat# PABG1-20, RRID:AB_2749857
Mouse monoclonal anti-H3K27me2/3	Active Motif	Cat# 39535; RRID:AB_2793246
Rabbit polyclonal anti-H3K9me3	Active Motif	Cat# 39161; RRID:AB_2532132
Mouse polyclonal anti-H3K9me3	Active Motif	Cat# 39161; RRID:AB_2935892
Mouse monoclonal anti-H4K20me1	Active Motif	Cat# 39285; RRID:AB_2615074
Mouse monoclonal anti-DNA	Millipore	Cat# MAB030; RRID: AB_93965
Rabbit polyclonal anti-H3K9ac	Abcam	Cat# ab10812; RRID: AB_297491
Rabbit polyclonal anti-H3K27ac	Active Motif	Cat# 39133; RRID: AB_2561016
Rabbit polyclonal anti-phospho-Histone H3 (Ser10)	Millipore	Cat# 06-570, RRID:AB_310177
Rabbit monoclonal anti-phospho-Histone H3 (Thr3) (clone JY325)	Millipore	Cat# 04-746, RRID:AB_11213949
Rabbit monoclonal anti- Lamin A/C	Abcam	Cat# ab108595; RRID: AB_10866185
Mouse monoclonal anti- Retinoblastoma (clone G3-245)	BD Biosciences	Cat# 554136; RRID:AB_395259
Rabbit monoclonal anti-Phospho-Rb (Ser807/811) (D20B12)	Cell Signalling	Cat# 8516; RRID: AB_11178658
Rabbit monoclonal anti-Rb (phospho T373) [EP821Y]	Abcam	Cat# ab52975; RRID: AB_2177344
Rabbit polyclonal anti-CDCA2	Abcam	Cat# ab45129; RRID: AB_869084
Mouse monoclonal anti-p21	BD Biosciences	Cat# 556430; RRID: AB_396414
Mouse monoclonal anti-p27Kip1	BD Biosciences	Cat# 610241; RRID: AB_397636
Mouse monoclonal anti-RNA polymerase II (F-12)	Santa Cruz Biotechnology	Cat# ab5131; RRID: AB_630203
Rabbit polyclonal anti-RNA polymerase II CTD repeat YSPTSPS (phospho S5)	Abcam	Cat# ab45129; RRID: AB_449369
Mouse monoclonal anti-DNA-RNA Hybrid Antibody (clone S9.6)	Millipore	Cat# MABE1095; RRID: AB_2861387
Mouse monoclonal anti- FBXO5	Thermo Fisher Scientific	Cat# 37-6600, RRID:AB_2533333
Mouse anti-CenpB	Earnshaw Lab	N/A
Guinea pig anti-CENP-C	MBL International	Cat# PD030, RRID:AB_10693556
Rabbit polyclonal anti-GFP	Abcam	Cat# ab290, RRID:AB_303395
Goat polyclonal anti-Mouse 800CW	LI-COR	Cat# 926-32210; RRID:AB_621842
Goat polyclonal anti-Rabbit 680RD	LI-COR	Cat# 926-68071; RRID:AB_10956166
Donkey polyclonal anti-Mouse polyclonal Alexa Fluor 594	Jackson Immunoresearch	Cat# 715-585-150; RRID:AB_2340854
Donkey polyclonal anti-Rabbit polyclonal Cy5	Jackson Immunoresearch	Cat# 711-175-152; RRID: AB_2340607
Donkey polyclonal anti-Mouse Cy5	Jackson Immunoresearch	Cat# 715-175-150; RRID:AB_2340819
Donkey polyclonal anti-Rabbit polyclonal Alexa Fluor 594	Jackson Immunoresearch	Cat# 711-585-152; RRID:AB_2340621
Donkey polyclonal anti-Guinea Pig Alexa Fluor 594	Jackson Immunoresearch	Cat# 706-585-148; RRID:AB_2340474

Developmental Cell
Resource

CellPress
OPEN ACCESS

Continued

REAGENT or RESOURCE	SOURCE	IDENTIFIER
Chemicals, peptides, and recombinant proteins		
3-Indoleacetic acid	Sigma-Aldrich	Cat# I2886; CAS:87-51-4
Thymidine	Sigma-Aldrich	Cat# T9250; CAS:50-89-5
Nocodazole	Sigma-Aldrich	Cat# M1404; CAS:31430-18-9
AZD1152-HQPA (Barasertib)	Bioquote	Cat# A10109; CAS:722544-51-6
Doxycycline	Sigma	Cat# D9891; CAS: 24390-14-5
Critical commercial assays		
Monarch Total RNA Miniprep Kit	New England BioLabs	Cat# T2010S
JetPrime®	Polyplus transfection®	Cat# 101000015
Deposited data		
RNA sequencing datasets	This paper	E-MTAB-13827
ATAC seq datasets	This paper	E-MTAB-13826
ChIP sequencing datasets	This paper	E-MTAB-15533
ChIP sequencing datasets PNUTS HeLa (GSM8413584, GSM8413578 and GSM8413579)	Bejjani et al.[28]	GSE272847
Proteomics data	This paper	PXD049319
Human reference genome GRCh38	Genome Reference Consortium Human Build 38	https://www.ncbi.nlm.nih.gov/assembly/GCF_000001405.26/
Experimental models: Cell lines		
HCT116:Ki-67-AID	Stamatiou et al.[26]	N/A
HCT116:Ki-67-AID mCherry-DHB	Stamatiou et al.[26]	N/A
HCT116:Ki-67-AID mCherry-GEMININ	Stamatiou et al.[26]	N/A
HCT116:Repo-Man-AID	This paper	N/A
HCT116:Repo-Man -AID mCherry-DHB	This paper	N/A
HCT116:Repo-Man -AID mCherry-GEMININ	This paper	N/A
HCT116:PNUTS-Man-AID	This paper	N/A
HCT116:PNUTS-AID mCherry-DHB	This paper	N/A
HCT116:PNUTS-AID mCherry-GEMININ	This paper	N/A
Oligonucleotides		
See Table S1 for Oligonucleotides used in this study	This paper	N/A
Recombinant DNA		
pX330-U6-Chimeric_BB-CBh-hSpCas9	Ran et al.[83]	Addgene plasmid #42230
pMK289 (mAID-mClover-NeoR)	Natsume et al.[84]	Addgene plasmid #72827
pMK290 (mAID-mClover-Hygro)	Natsume et al.[84]	Addgene plasmid #72828
pMSCV-Blasticidin	Kendall et al.[85]	Adgene plasmid #75085
CSII-pEF-hDHB-mCherry	Laboratory of Dr Steven D. Cappell (Center for Cancer Research National Cancer Institute,USA)	N/A
CSII-pEF-hGEMININ-mCherry	Laboratory of Dr Steven D. Cappell (Center for Cancer Research National Cancer Institute,USA)	N/A
pGEM-T Easy-Repo-Man- mAID-mClover-Neo	This paper	N/A
pGEM-T Easy-Repo-Man – mAID-mClover-Hygro.	This paper	N/A
pX330-U6-Chimeric-BB-CBh-hSpCas9-gRNA-Repo-Man-P1	This paper	N/A

(*Continued on next page*)

Continued

REAGENT or RESOURCE	SOURCE	IDENTIFIER
pX330-U6-Chimeric-BB-CBh-hSpCas9-gRNA-Repo-Man -P2	This paper	N/A
pX330-U6-Chimeric-BB-CBh-hSpCas9-gRNA-Repo-Man -P3	This paper	N/A
pBluescript II SK(+)-PNUTS- mAID-mClover-Neo	This paper	N/A
pBluescript II SK(+)-PNUTS- mAID-mClover-Hygro.	This paper	N/A
pX330-U6-Chimeric-BB-CBh-hSpCas9-gRNA-PNUTS-P1	This paper	N/A
pX330-U6-Chimeric-BB-CBh-hSpCas9-gRNA-PNUTS-P2	This paper	N/A
pX330-U6-Chimeric-BB-CBh-hSpCas9-gRNA-PNUTS-P3	This paper	N/A
Software and algorithms		
ImageJ	Schneider et al.[86]	https://imagej.nih.gov/ij/
Samtools	Li et al.[87]	http://samtools.sourceforge.net/
HTSeq	Anders et al.[88]	https://htseq.readthedocs.io/en/master/
Deseq2	Love et al.[89]	https://bioconductor.org/packages/release/bioc/html/DESeq2.html
NIS-Elements	Nikon	N/A
SoftWoRx	Delta Vision	N/A
R studio		https://posit.co/
MaxQuant software platform	Cox and Mann[90]	N/A
Andromeda search engine	Cox et al.[91]	N/A
Deeptools	Ramírez et al.[92]	N/A
Bedtools	Quinlan and Hall[93]	N/A
Recognicer	Zang et al.[94]	N/A

EXPERIMENTAL MODEL AND STUDY PARTICIPANT DETAILS

Cell lines

The HCT116 cell line stably expressing OsTIR1 under TET-ON promoter (HCT116-TET-OsTIR1) was kindly provided by Dr Masato T. Kanemaki (University of Tokyo, Japan) and used to generate the cell lines used in the study. HCT116 cells were grown in McCoy's 5A Medium GlutaMAX (Gibco) supplemented with 10% foetal bovine serum (FBS) (Labtech), 100 U/mL penicillin and 100 μg/mL streptomycin (Gibco) in a humidified incubator at 37°C with 5% CO2.

HCT116-Ki-67-mAID-mClover-HygR/NeoR, HCT116-Ki-67-mAID-mClover-HygR/NeoR + DHB-mCherry and HCT116-Ki-67-mAID-mClover-HygR/NeoR + GEMININ-mCherry cell lines were generated in the Vagnarelli's lab as previously described (DOI: https://doi.org/10.1101/2023.04.18.537310). They were not authenticated as unique and recognizable by the specific localization of the endogenous GFP-tagged alleles, and the ability to degrade the protein upon addition of IAA and doxycyclin.

METHOD DETAILS

Plasmids

pX330-U6-Chimeric_BB-CBh-hSpCas9 (no. 42230, Addgene) plasmids containing guide RNAs (gRNAs), designed with CRISPOR (http://crispor.tefor.net), were generated according to.[83] The sequences of gRNAs are listed in Table S1.

To generate the plasmid donors containing Repo-Man or PNUTS homology arms, genomic DNA from HCT116-TET-OsTIR1 cells was purified by using EchoLUTION CellCulture DNA Kit (BioEcho), and the genomic DNA region around the stop codon of Repo-Man (1.2 kb) or PNUTS (1.3 kb) was amplified using Phusion High-Fidelity DNA Polymerase (Thermo Fisher Scientific; primers are listed at Table S1), cloned into pGEM-T Easy empty vector (Promega) and sequenced. Based on sequencing, plasmids containing Repo-Man or PNUTS homology arms were synthesized, with the following changes: the stop codon was mutated into a BamHI restriction site and silent point mutations were introduced within PAM sequences. The mAID-mClover-HygR (hygromycin resistance) cassette and mAID-mClover-NeoR (neomycin resistance) cassette[84] were then inserted into the BamHI site, in frame with Repo-Man or PNUTS to generate homology arms donor plasmids.

Developmental Cell
Resource

Cell line generation

For the generation of Repo-Man/PNUTS-mAID-mClover-HygR/NeoR cell lines, HCT116-TET-OsTIR1 cells were transfected with 2 µg of total DNA of pX330-U6-Chimeric_BB-CBh-hSpCas9 and homology arms plasmids (Repo-Man-mAID-mClover-HygR and Repo-Man-mAID-mClover-NeoR or PNUTS-mAID-mClover-HygR and PNUTS-mAID-mClover-NeoR for mAID cell lines; or -APEX2-mClover-HygR and -APEX2-mClover-NeoR for APEX cell lines) in 1:1:1 ratio, and selected for 14 days with 100 µg/mL hygromycin B (10687010, Invitrogen) and 700 µg/ml of geneticin (10131027, Gibco). Clones were first assessed by microscopy and then screened via PCR genotyping using 3-5 different combinations of primers, which targeted sequences outside of homology arms and within tagging inserts (Table S1: List of oligonucleotides used in the study).

For the generation of HCT116-Repo-Man/PNUTS-mAID-mClover-HygR/NeoR + DHB-mCherry stable cell lines, HCT116-Repo-Man/PNUTS-mAID-mClover-HygR/NeoR cells were co-transfected with 2 µg of total DNA of CSII-pEF-hDHB-mCherry and pMSCV-Blasticidin in 9:1 ratio and selected with 10 µg/ml blasticidin (15205, Merck). Clones were chosen by microscopy.

For the generation of HCT116-Ki-67/Repo-Man/PNUTS-mAID-mClover-HygR/NeoR + Geminin-mCherry stable cell lines, the same process was followed as the DHB-mCherry cell line generation.

Mitotic synchronisation and protein degradation for G1 analyses

Unless stated otherwise, HCT116 cells (Ki-67 or Repo-Man or PNUTS-mAID-mClover-HygR/NeoR) were treated with 2 µg/ml doxycycline (D9891, Merck) and 0.06 µg/ml nocodazole (M1404, Merck), 24 and 18 h respectively, before the addition of 1 mM IAA (I2886, Merck) to induce degradation of mAID-tagged proteins. After 4 h treatment with IAA, mitotic cells were manually detached by shake-off, and cells were transferred to new poly-L-lysin coated dishes. Once attached, cells were washed 3x with phosphate buffered saline (PBS) and released from mitosis into G1 for 18 h in a fresh medium containing 2 mM thymidine (T9250, Merck).

Immunofluorescence microscopy

Cells were fixed with 4% paraformaldehyde (PFA; 10131580, Fisher Scientific) in PBS, for 5 minutes followed by 3x washes with 1X PBS (Severn Biotech). The cells were then permeabilized with 0.2% Tritox-X for 2 minutes at room temperature (RT) then incubated in blocking buffer (1% BSA in PBS) for 30 min at 37°C. The primary antibody was diluted in blocking buffer, at the dilution recommended for each antibody, added to the coverslips and incubated for 30 min at 37°C covered with parafilm. After 3x washes in PBS, the secondary antibody was added at 1:500 dilution in blocking buffer and incubated for 30 min at 37oC covered with parafilm. Finally, the cells were mounted with Vectashield mounting media (Vector Laboratories) containing DAPI. Primary and secondary antibodies used in the study are listed in key resources table. Three-dimensional data sets were acquired using a wide-field microscope (Delta Vision) Cascade II:512 camera system (Photometrics) and a wide-field microscope (NIKON Ti-E super research Live Cell imaging system) with a 100X Plan Apochromat lens, numerical aperture (NA) 1.45. The data sets were deconvolved using Delta Vision software or Nikon NIS element. Three-dimensional data sets were converted to a maximum projection, exported as PNG files and imported into Inkscape software (version 0.91) for final presentation.

For deepSIM imaging a NIKON Ti2-E inverted microscope with 100X Plan Apochromat lens, numerical aperture (NA) 1.45 with Teledyne Photometrics Kinetix camera. 3D stacks were acquired and reconstructed with the NIS software.

Immunoblotting

Whole-cell extracts were prepared by direct lysis in 1x Laemmli sample buffer.

For histone isolation, HCT116 cells were synchronised, proteins of interest were degraded as described above and collected at the G1 stage of the cell cycle. 5x10^6 cells were collected from each condition and incubated for 10 min on ice with 500 µl lysis buffer (1 mM Tris-HCl, pH 7.5, 10 mM NaCl, 0.5% NP-40) supplemented with protease and phosphatase inhibitors. After 3 min centrifugation at 1,000 g at 4°C, the supernatant was discarded, the pellet was resuspended in 500 µl lysis buffer and samples were pelleted again as above. The pellet was flash-frozen in liquid nitrogen and stored at -20°C for 1 h. Next, the pellet was thawed on ice for 15-30 min and washed with 400 µl of digestion buffer (50 mM Tris-HCl, pH 7.5, 1 mM CaCl2, 4 mM MgCl2, 300 mM sucrose). After 10 min centrifugation at 100 g at 4°C, the supernatant was discarded, and the pellet was resuspended in 300 µl of digestion buffer with 600 U of micrococcal nuclease (MNase) (M0247, New England Biolabs) and incubated for 30 min at 37°C. The MNase reaction was terminated by adding 1mM EDTA. The digested sample was then centrifugation for 20 min at 8,000 g at room temperature (RT) and the pellet was resuspended in 1x Laemmli sample buffer.

The proteins were separated by SDS–PAGE and transferred onto nitrocellulose membranes (10600003, Amersham). Membranes were blotted with primary and secondary antibodies, which are listed in Table S2, and visualised using the LiCor Odyssey system or g-Box Chemi Xrq Gel Doc System.

CDK2 activity analyses

HCT116 cell lines containing mAID-tagged proteins and stably-expressed DHB-mCherry were synchronised, and proteins were degraded as described above. Upon reaching the G1 stage of the cell cycle, cells were fixed with 4% PFA in PBS. Coverslips were mounted with VECTASHIELD® Antifade Mounting Medium (H-1000-10, Vector Laboratories) containing DAPI, and observed on a wide-field microscope (NIKON Ti-E super research Live Cell imaging System). The analysis of CDK2 activity was performed in ImageJ, where the nuclear and cytoplasmic signal intensities of DHB–mCherry were quantified. The ratio of cytoplasmic to nuclear

DHB–mCherry signal was calculated for each cell and subsequently used to generate violin plots in RStudio. Violin plots were generated with R Studio. The Wilcoxon statistical analysis was conducted with R Studio.

APC/C activity analyses

HCT116 cell lines containing mAID-tagged proteins and stably-expressed Geminin-mCherry were treated as DHB-mCherry-expressing cells described above. The analysis of APC/C activity was performed in Fiji, quantifying the proportion of cells exhibiting active APC/C (Geminin–mCherry not detected) and inactive APC/C (Geminin–mCherry detected). The number of cells in each category was recorded, and the corresponding percentages were calculated. Violin plots were generated with R Studio. The Wilcoxon statistical analysis was conducted with R Studio.

Comet assay

The alkaline comet assay was adapted from (Tice et al., 2000[95]). Poly-L-lysine coated slides were first covered with 1% high-melting-point agarose and dried overnight at room temperature. After cell treatment, a drop of normal-melting-point agarose was first loaded on a slide, and then a drop of low-melting-point agarose was put on the precoated slide. Then, 104 cells were placed in the agarose droplet. Slides were lysed in a detergent solution (containing 2% N-Lauroylsarcosine sodium salt, 0.5 M Na2EDTA and 0.1 mg/ml proteinase K), for 1 hour at 4°C. DNA unwinding was carried out with a neutral solution at pH 8.5 (90 mM Tris-HCl, 90 mM boric acid and 2 mM Na2EDTA) for 90 minutes at RT in a 1-L electrophoresis unit. Electrophoresis was conducted for 40 minutes (20 V) in the same buffer solution at 4oC. After the electrophoretic run, the slides were neutralized with distilled water, stained with SYBR Safe in TE buffer, dehydrated by dipping into 70%, 90% and 100% ethanol, sequentially, and then dried overnight at RT. Images were captured using Leica DM4000 fluorescence microscope (Leica Microsystems). Comet length was measured in ImageJ.

Fluorescence in situ hybridisation (FISH)

HCT116 cells with mAID-tagged proteins were synchronised and protein degraded as described above. Cells were fixed twice as follows: 15 min with 75 mM KCl, then 30 min with 3:1 ice-cold methanol:acetic acid. Finally, cells were stored in methanol/acetic acid at -20°C. P1-derived artificial chromosome (PAC)-derived probes were extracted from bacterial cultures and fluorescently labelled by nick translation using Nick Translation Kit (Abbott), following the manufacturer's instructions. The probe was separated using G-50 column, precipitated at -20°C in the presence of 3μg salmon sperm DNA and 3 M sodium acetate (10% of the volume of the probe), and 2 volumes of 100% EtOH were added to precipitate the probe for 24h at -20oC. The probes were centrifuged at 10,000 g for 30 min at 4°C. The supernatant was removed, and the pellet was dried for 10 - 15 minutes. Finally, the probes were resuspended in 30μl purified waterfor the centromeric probes.

Pericentromeric/α-satellite FISH

The probe (3 μl of probe and 7 μl of hybridisation buffer: 50% (v/v) formamide, 10% (w/v) dextran sulphate, 1x Denhart's, 2x SSC, pH 7.0) was denatured at 73°C for 5 min. Probe and nuclei were denatured at 85°C for 5 min, and then hybridised overnight at 39°C. Slides were washed with 2x SSC at RT for 10 min, 0.4x SSC at 60°C for 10 min, 0.1x SSC at RT for 10 min and counterstained with DAPI.

For all FISH analyses, three-dimensional data sets were acquired using a wide-field microscope (NIKON Ti-E super research Live Cell imaging system) with 100x, 1.45 (NA) Plan Apochromat lens. The data sets were deconvolved with NIS Elements AR analysis software (NIKON). Three-dimensional data sets were converted to maximum projection in the NIS software, exported as TIFF files, and imported into Inkscape software (version 0.91) for final presentation.

Proximity ligation assay (PLA)

Proximity ligation assay was performed according to the manufacturer's protocol (Sigma). HCT116:Ki-67-AID cells were treated as indicated in Figure 1A or with Doxycycline (2μg/ml) and 0.06 μg/ml Nocodazole for 24 and 18 h before the addition of IAA 1000μM, respectively. After the completion of the experiment indicated in Figure 1A or 4 h treatment with IAA the cells were fixed, permeabilized and blocked with BSA as described in the immunofluorescence microscopy section. The antibodies were used at a concentration as follows, 1:1000 anti-CENP-B (gift from W.C. Earnshaw, Edinburgh) and 1:10,000 anti-GFP [PABG1] (Cat# PABG1-20, RRID:AB_2749857). PLA probes were added, and ligation was performed following the manufacturer instructions (Sigma). Coverslips were mounted with vectashield containing DAPI and observed on the previously mentioned wide-field NIKON microscope.

RNA sequencing

Total RNA was extracted from HCT116 cells, with or without the protein of interest following the experiment described in Figure 1A, using Monarch Total RNA Miniprep Kit (New England Biolabs), according to manufacturer's instructions. RNA samples were sent to Macrogen Europe B.V (The Netherlands). Macrogen Europe BV constructed libraries using Illumina TruSeq stranded mRNA library preparation with Ribozero rRNA depletion. Sequencing was performed with a Novaseq 6000 platform, at 100 M paired-end reads per sample.

The trimmed reads were aligned to the human reference genome GRCh38, using HISAT2 (v2.2.1) under standard conditions.

Developmental Cell
Resource

The resulting alignments were filtered for high quality hits using SAMtools v0.1.12[87] with a minimum selection threshold score of 30. FeatureCounts function (from Subread package v2.0.2) was used to count gene level reads, and Deseq2 was used to identify differentially expressed genes between samples and calculate the Pearson correlation.

The differential expression was expressed in the form of log2 fold change between sample and control and deemed statistically significant by a lower p-value of 0.05.

Functional enrichment was analysed using STRING (string-db.org), while Venn diagrams were performed in the free software FunRich. Volcano plots were performed using the ggplot package (v3.4.2) in R Studio.

ATAC sequencing
Synchronised HCT116:RIPPOs-AID cells, with or without IAA were used following the experiment described in Figure 1A. For each cell line, two replicates containing 100,000 cells per condition were submitted to Active Motif for ATAC-sequencing.

Alignment of the ATAC-seq data was performed against the human reference genome GRCh38. Peaks calling was made using MACS 2.1.0 with 1e-7 as cut-off of p-value, without control file and with the -nomodel parameter. Peaks were filtered using the ENCODE blacklisted regions. FRIP (fraction of reads in peaks) value for each sample is higher than 25%.

Bioconductor (v3.16) packages DiffBind and DESeq2 were used to identified differentially accessible regions between samples. ChIP-seq datasets for H3K9ac and H3K27ac were downloaded from the public database ENCODE (ENCFF105NDA and ENCFF853VVI, respectively). Overlaps between the differentially accessible region identified in our ATAC-seq dataset and H3K9ac or H3K27ac ChIP-seq datasets were identified with bedtools 2.31.0. Statistical significance of these overlaps was given by Fisher's test (fisher function with bedtools).

Hg38 Repeat file was downloaded from UCSC Genome browser (https://genome.ucsc.edu) and overlaps between the differentially accessible region identified in our ATAC-seq dataset and the repeat dataset was made using bedtools 2.31.0. Statistical significance of these overlaps was given by Fisher's test (fisher function with bedtools).

Pearson correlation
Correlation plots were constructed on Pearson correlation values between replicates using corrplot (v.095) in R environment.

Mass spectrometry
Protein samples were processed at the same time and using the same digestion protocol without any deviations. They were subjected for MS analysis under the same conditions. Protein and peptide lists generated using the same software and the same parameters. Specifically, 30 µg of total protein from each sample were digested using the Filter Aided Sample Preparation (FASP) protocol as described by (Wisniewski et al., 2009[96]) with minor modifications. In brief, each protein sample was added on the top of a 30 kDa MWCO filter units (Vivacon, UK) along with 150 µl of denaturation buffer (8M Urea in 50mM ammonium bicarbonate (ABC) (Sigma Aldrich) and spun at 14,000 x g for 20 min, while another wash with 200 µl of denaturation buffer was performed under the same conditions. The protein samples were then reduced by the addition of 100 µl of 10 mM dithiothreitol (Sigma Aldrich, UK) in denaturation buffer for 30 min at ambient temperature, and alkylated by adding 100 µl of 55 mM iodoacetamide (Sigma Aldrich, UK) in denaturation buffer for 20 min at ambient temperature in the dark. Two washes with 100 µl of denaturation buffer and two with digestion buffer (50mM ABC) were performed under the same conditions described above before the addition of trypsin (Pierce, UK). The protease:-protein ratio was 1:50 and proteins were digested overnight at 37°C. Following digestion, samples were spun at 14,000 x g for 20 min and the flow-through containing digested peptides was collected. Filters were then washed one more time with 100 µl of ABC and the flow-through was collected again. The eluates from the filter units were acidified using 20 µl of 10% Trifluoroacetic Acid (TFA) (Sigma Aldrich, UK), and 2% of the eluate was spun onto StageTips as described by (Rappsilber et al., 2007[97]). The rest 98% of the eluate was subjected to phospho-enrichment using Ti-IMAC MagResyn® beads (ReSyn Biosciences), following the beads' protocol without deviations. Following enrichment, peptides were concentrated and cleaned using the same StageTip protocol as above.

In both cases, peptides were eluted in 40 µL of 80% acetonitrile in 0.1% TFA and concentrated down to 1 µL by vacuum centrifugation (Concentrator 5301, Eppendorf, UK). The peptide sample was then prepared for LC-MS/MS analysis by diluting it to 5 µL by 0.1% TFA.

LC-MS analyses were performed on an Orbitrap Exploris™ 480 Mass Spectrometer (Thermo Fisher Scientific, UK) coupled on-line, to an Ultimate 3000 HPLC (Dionex, Thermo Fisher Scientific, UK). Peptides were separated on a 50 cm (2 µm particle size) EASY-Spray column (Thermo Scientific, UK), which was assembled on an EASY-Spray source (Thermo Scientific, UK) and operated constantly at 50oC. Mobile phase A consisted of 0.1% formic acid in LC-MS grade water and mobile phase B consisted of 80% acetonitrile and 0.1% formic acid. Peptides were loaded onto the column at a flow rate of 0.3 µL min-1 and eluted at a flow rate of 0.25 µL min-1 according to the following gradient: 2 to 40% mobile phase B in 120 min and then to 95% in 11 min. Mobile phase B was retained at 95% for 5 min and returned back to 2% a minute after until the end of the run (160 min).

Survey scans were recorded at 120,000 resolution (scan range 350-1500 m/z) with an ion target of 3.0e6, and injection time of 50ms and RF lens of 40%. MS2 was performed in the orbitrap in Data Dependent Acquisition (DDA) mode at 15,000 resolution with isolation window of 1.4, maximum injection time of 50ms and AGC target of 8.0E5 ions. We used HCD fragmentation (Olsen et al., 2007[98]) with stepped collision energy of 30. Data for both survey and MS/MS scans were acquired in profile mode.

The MaxQuant software platform[90] version 1.6.1.0 was used to process the raw files from the SILAC labelled samples and the search was conducted against the complete/reference proteome set of Homo sapiens (Uniprot database - released in 2019), using

the Andromeda search engine.[91] For the first search, peptide tolerance was set to 20 ppm while for the main search peptide tolerance was set to 4.5 pm. Isotope mass tolerance was 2 ppm and maximum charge to 7. Digestion mode was set to specific with trypsin allowing maximum of two missed cleavages. Carbamidomethylation of cysteine was set as fixed modification. Oxidation of methionine and phosphorylation of serine, threonine and tyrosine were set as variable modifications. To account for the SILAC labels, multiplicity was set to 2, with lysine +8 and arginine +10 selected. FDR was set to 1%.

Chromatin immunoprecipitation (ChIP)

HCT116 and HCT116:Repo-Man-AID and HCT116:Ki67-AID cell lines were cultured in 15 cm dishes and treated for 18 h with 2 mM thymidine. Cells were harvested as follows: after removing the medium, cells were washed once with phosphate-buffered saline (PBS) containing 1 mM phenylmethylsulfonyl fluoride (PMSF) and 1 mM CLAP protease inhibitor and fixed using 1% formaldehyde in PBS containing 1 mM PMSF and 1 mM CLAP for 7 minutes at room temperature (RT). Fixation was quenched with 0.125 M glycine in PBS for 5 minutes on ice. Cells were scraped, pelleted by centrifugation at 1,000×g for 5 minutes, washed twice with 5 mL ice-cold PBS containing 1 mM PMSF and 1 mM CLAP, snap-frozen in liquid nitrogen, and stored at −80°C.

Pelleted cells were resuspended in 2 mL ChIP Buffer I (50 mM HEPES pH 7.6, 140 mM NaCl, 1 mM EDTA pH 8.0, 0.5 mM EGTA pH 8.0, 10% glycerol, 0.5% NP-40, 0.25% Triton X-100, 1 mM PMSF, and 1 mM CLAP) and incubated on a rotator at 4°C for 15 minutes. Cells were pelleted by centrifugation at 1,000×g for 5 minutes, resuspended in ChIP Buffer II (20 mM Tris-HCl pH 8.0, 200 mM NaCl, 1 mM EDTA pH 8.0, 0.5 mM EGTA pH 8.0, 1 mM PMSF, and 1 mM CLAP), and incubated on a rotator at 4°C for 10 minutes. Following another centrifugation step (1,000×g, 5 minutes), the pellet was resuspended in ChIP Buffer III (20 mM Tris pH 8.0, 100 mM NaCl, 1 mM EDTA pH 8.0, 0.5 mM EGTA pH 8.0, 0.5% Sarkosyl, 0.1% sodium deoxycholate (NaDOC), 1 mM PMSF, and 1 mM CLAP). Cells were sonicated using a Bioruptor (50 cycles of 30 seconds ON/30 seconds OFF). Triton X-100 was added to the lysate to achieve a final concentration of 1%. Lysates were clarified by centrifugation at 16,000×g for 10 minutes, and the supernatant was transferred to fresh tubes and stored at −80°C. A 100 μL aliquot was reserved from each sample for input controls.

For immunoprecipitation, lysates were incubated overnight with 25 μg anti-GFP antibody, followed by a 4-hour incubation with 150 μL protein G magnetic Dynabeads (Invitrogen) per immunoprecipitation (IP). Beads were sequentially washed with 1 mL of the following buffers for 5 minutes at 4°C with rotation: Low-Salt Wash Buffer (20 mM Tris-HCl pH 8.0, 150 mM NaCl, 2 mM EDTA pH 8.0, 0.1% SDS, and 1% Triton X-100), High-Salt Wash Buffer (20 mM Tris-HCl pH 8.0, 500 mM NaCl, 2 mM EDTA pH 8.0, 0.1% SDS, and 1% Triton X-100), and LiCl Buffer (10 mM Tris-HCl pH 8.0, 250 mM LiCl, 1% IGEPAL, 1% NaDOC, and 1 mM EDTA pH 8.0). Beads were washed twice with TE buffer and resuspended in 200 μL TE buffer.

To remove RNA, RNase A was added to a final concentration of 0.33 mg/mL, and samples were incubated at 37°C for 1 hour. Proteinase K was added to a final concentration of 0.5 mg/mL, followed by incubation at 56°C for 2 hours and overnight decrosslinking at 56°C. DNA was separated from the magnetic beads, purified using AMPure XP beads (according to the manufacturer's protocol), and quantified using a Qubit fluorometer.

ChIP sequencing was conducted from Novogene using NEBNext® Ultra™ IIDNA Library Prep Kit (Cat No. E7645), and sequencing platform Illumina NovaSeq X Plus Series.

ChIP-seq analysis

Sequences were aligned to human genome Hg38 with bowtie2 (Langmead and Salzberg, 2012) with default parameters. High quality primary alignments were selected with samtools view with the parameters -F 260 and -q 20, and duplicates marked with samtools markdup (Danecek et al., 2021[99]). Bigwig profiles were generated at 500 bp resolution with Deeptools bamCoverage for each individual sample and bigwigCompare for IP vs input profiles, using the RPGC (reads per genomic content) and SES (signal extraction scaling) normalisation methods respectively.[92]

Domains were determined using Recognicer with parameters -w 500 -fdr 10e-6–step_size 20 –step_score 12.[94]

Co-occupancy analysis

The human genome was divided into 5 kb bins with bedtools window. Each bin was intersected with the peak sets from Repo-man, Ki-67 and PNUTS using bedtools closest,[93] The number of bins that intersect each combination of proteins were then counted.

Analysis of publicly available datasets

DamID datasets were retrieved from GEO (GSE186206 for Ki-67; GSE54170 for Repo-Man and PNUTS). Bed files with genomic coordinates were filtered for UCSC annotated promoter regions using GenomicRanges (v.1.60.0) and annotated (v.1.34.0) in R environment. Annotated promoter regions as GRanges were intersected for overlaps by Venn diagrams (VennDiagram v.1.7.3).

QUANTIFICATION AND STATISTICAL ANALYSES

FISH analyses

For the signal area analyses, 3D stack images were exported and analysed with ImageJ. Scale was set to 1 μm, ROIs of the signals were created using threshold function and wand tracing tool, the area in μm was used to generate the violin plots.

Developmental Cell
Resource

CENP-B

Quantification of the kinetochore/centromere staining. CENP-B, 3D stack images of control and Ki-67-degraded cells; were exported and analysed with the Foci quantification plug-in using Fiji (1_color_auto.ijm) (Ledesma-Fernandez and Thorpe, 2015). Background was subtracted, and the mean intensity was used to generate the violin plots.

PLA

Spots laying within nuclear masks were counted in control and Ki-67-degraded cells; the numbers of foci were used to generate the violin plots.

Nuclear area

For the signal area analyses, 3D stack images were exported and analysed with ImageJ. Scale was set to 1 μm, ROIs of the nuclear area were created, the area in μm was used to generate the violin plots.

RNA Polymerase II (POL II)

For each HCT116 cell line (Ki-67 or Repo-Man or PNUTS), images were acquired for three biological replicates using a wide-field microscope (NIKON Ti-E super research Live Cell imaging system) with 40x, 1.45 (NA) Plan Apochromat lens. Analysis was then conducted in NIS Elements AR analysis software (NIKON). Using nuclei as a mask, fluorescent intensities of RNA POL II and phospho-S5-RNA POL II were measured. Background of each channel from each image w subtracted and the ratio of fluorescence intensity of phospho-S5-RNA POL II/total RNA POL II was used to generate the violin plots

Statistical analyses

Statistical analyses were performed either in Excel (chi-squared test) or in R (using the Wilcoxon rank test function, differential expression, lowest smoothing).